Project information	
Project full title	EuroSea: Improving and Integrating European Ocean Observing and Forecasting Systems for Sustainable use of the Oceans
Project acronym	EuroSea
Grant agreement number	862626
Project start date and duration	1 November 2019, 50 months
Project website	https://www.eurosea.eu

Deliverable information	
Deliverable number	5.11
Deliverable title	**Scientific model validation report during the demonstration period**
Description	Validation of coastal models with existing and new monitoring instruments during the last 6-months of the project
Work Package number	5
Work Package title	Coastal Resilience and Operational Services Demonstrator
Lead beneficiary	Puertos del Estado, EPPE
Lead authors	Pablo Lorente Jiménez, Begoña Pérez Gómez, Ivan Federico, Anna Matulka, Angela Hibbert, María Liste
Contributors	Susana Pérez Rubio, Simon Williams, Giovanni Copini, Marc Mestres, Manuel Espino
Due date	31.12.2023
Submission date	22.12.2023
Comments	

This project has received funding from the European Union's Horizon 2020 research and innovation programme under grant agreement No. 862626.

https://doi.org/10.3289/eurosea_d5.11

Table of contents

Executive summary

The skills assessment of high-resolution coastal models developed within the OSPAC (Oceanographic Services for Ports and Cities) demonstrator for Barcelona and Taranto pilot sites has shown positive performance during the August-December 2023 demonstration phase. Comparisons with observational data from new sensors and permanent stations, operationally integrated in OSPAC tool during that period, as well as offline validation exercises from earlier data periods, validate the models' accuracy. The GNSS-IR technique, utilizing both low-cost and high-precision GNSS sensors, demonstrated its potential for providing significant wave height values at the coast.

In Barcelona, the wave model revealed consistent model performance, despite overestimating certain wave height events. Hydrodynamic modulations by underlying currents were identified as a factor requiring further investigation into waves–current interactions. A 3-month multi-parameter intercomparison for two coastal ocean models (with and without waves-currents coupling) around Barcelona harbour showed robust performance in both cases, capturing events like Storm Babet's sea level rise. Notably, the coupled model did not outperform the non-coupled model, suggesting the need for the extension of model intercomparison in the future to longer periods including diverse oceanic and meteorological conditions and significant extreme events.

In Taranto, the first day of forecasts is validated against the new sea level and significant wave height data provided by EuroSea tide gauge. For sea level, the results are comparable to the findings of the hindcast validation in previous studies. Regarding the significant wave height, the model shows satisfactory agreement with the two new sources of in situ waves information provided by EuroSea tide gauge, despite overestimating one of the wave peaks observed in the period.

The study highlights the effectiveness of a combined observational and modelling approach for comprehensive coastal processes characterization, leveraging the strengths of both systems.

1. Introduction

The main goal of the present document is to showcase the ocean modelling and observational components currently working in place around Taranto and Barcelona harbours, in the frame of the OSPAC (Oceanographic Services for Ports and Cities) demonstrator at the two pilot sites (Deliverables 5.3, 5.4, 5.5, 5.9 and 5.10). A scientific validation of the new developed high-resolution coastal models is performed for the last 6 months of the project, corresponding to the demonstration period, with all data streams from EuroSea new equipment and other permanent instrumentation entering OSPAC tool in an operational way. An offline validation during the model implementation with other in situ observations from temporal campaigns was already presented in Deliverables 5.3[1] and 5.4[2].

For the specific case of Barcelona, two different exercises were conducted:

[1] https://doi.org/10.3289/eurosea_d5.3
[2] https://doi.org/10.3289/eurosea_d5.4

i. A wave model-observation validation exercise for the period June-November 2023 was performed, in order to evaluate de performance of the high-resolution coastal wave model, developed in the project and running operationally in EPPE, to meet Barcelona harbour operator´s needs.
ii. A numerical investigation with a new coupled model (where the combined wave-current interactions were considered) has been performed. To this end, a multi-parameter inter-comparison of two similar coastal forecast models (without coupling and with coupling) was conducted at the sea surface for a 3-month period (September-November 2023) in order to evaluate de performance of both high-resolution coastal models running operationally in EPPE and assess the potential added-value of the coupling approach.

For Taranto, an assessment of the modelling skills against the new data from the EuroSea equipment installed in this harbour was made for the period ranging from September 2023 (installation) to the end of November 2023, for the variables significant wave height and sea level.

The report is organized as follows: Section 2 presents an overview of the observational data used for the validation at the two pilot sites, and Section 3 describes the main characteristics of the corresponding modelling components. Section 4 explains the methodology, model data and metrics used for the validation process, and Section 5 presents the validation results.

2. Observational data

Description of the equipment and observational data available for the two pilot sites is presented in this section. Apart from the new equipment installed in the frame of EuroSea, data from other permanent stations in the port of Barcelona, also integrated in OSPAC, have been included in the validation exercise. More details about the new stations deployed in the frame of the project can be found in *Deliverable 5.9: Operational monitoring systems available at the three sites.*

2.1. Barcelona pilot site

The following stations have been used for Barcelona validation exercise of the waves and circulation models (positions displayed in Figures 1 and 2).

Barcelona II coastal buoy

A Directional Triaxis buoy was moored at 68 m depth in March 2004, close to Barcelona harbour (2.20°E-41.32°N). This in situ device, operated by EPPE, collects hourly-averaged estimations of diverse wave, encompassing the significant wave height (SWH_o), maximum wave height (MWH_o), mean period (Tmo), peak period (Tp_o) and incoming mean wave direction (MWD_o). The quality control applied to data time series, defined by the Copernicus Marine In situ Team (Copernicus Marine In situ Team, 2017), consisted of a battery of automatic checks performed to flag and filter inconsistent values. For the Mediterranean Sea, the spike test was based on the difference between sequential measurements of SWH_o, Tm_o, and Tp_o so they were discarded, respectively, when the difference exceeded 3 m, 4 s and 10 s. Occasional gaps (not larger than 6 h) were linearly interpolated to ensure the continuity of the records.

Barcelona II tide gauge

A radar tide-gauge, manufactured by Miros and operated by EPPE as part of its REDMAR network (Pérez Gómez et al., 2008 and 2014), was deployed inside of Barcelona harbour in October 2007 (2.17°E – 41.34°N, denoted in Figure 2c). Manufacturer claimed accuracy for sea level is +/- 1 mm. Quality-controlled 2 Hz sea

level data contain information of sea level oscillations with periods above 1 s, capturing all sea surface height variability including waves, high-frequency sea level oscillations and tides. In the present work, hourly estimations of total water fluctuations (SSH_o) were used to evaluate models' performance. Data have been quality controlled and processed by EPPE according to international best practices (UNESCO/IOC, 2020), including application of a filter to obtain hourly values (Pugh, 1987).

RAD1 and RAD2 tide gauges (EuroSea)

A new prototype low maintenance tide gauge system was developed by the NOC in the frame of EuroSea. Powered by renewable energy, the new station is based on dual sea level sensors and telemetry and has the ability to monitor both land motion and sea level by means of a co-located permanent GNSS (Global Navigation Satellite System) receiver. NOC engineers in collaboration with the Port Authority, SIDMAR Spanish company and EPPE completed the deployment and installation of this new tide gauge in Barcelona in April 2023, at the northern entrance of the harbour (2.19ºE – 41.36ºN). The two sea level sensors, used in this validation report, are YSI Waterlog Nigle 502 radar water levels sensors (RAD1 and RAD2), with manufacturer's reported accuracy of +/- 2 mm, recording 1 second samples averaged across 1 min. In the present work, hourly estimations of total water fluctuations (SSH_o) were used to evaluate models' performance. These sea level data have been quality controlled and processed by EPPE according to international best practices (UNESCO/IOC, 2020), including application of a filter to obtain hourly values (Pugh, 1987). Both sensors location is indicated in Figure 2c.

Low cost Global Navigation Satellite System - GNSS (EuroSea)

Between the novel multi-parametric equipment deployed at Barcelona pilot site in the frame of EuroSea, a new experimental technique known as GNSS Interferometric Reflectometry (GNSS-IR) is used to provide mean sea level and significant wave height. For the latter, a low cost Emlid REACH M2 GNSS antenna was installed at the northern entrance of the harbour, on the lighthouse, to measure SWH outside the harbour walls, where large swell waves can potentially affect navigation. The antenna collects 1-s samples of carrier phase, range, and signal-to-noise ratio. These data are then transmitted via a roaming SIM card at hourly intervals to the National Oceanography Centre (NOC) in the RINEX 3 format. Currently, these data are manually processed every few days using the IR technique mentioned above to generate hourly SWH estimates. The results are currently undergoing calibration, and there is a strong agreement between these observations and those obtained from the offshore buoy operated by EPPE.

Ancillary data

Hourly in situ estimations of wind speed and direction from a meteorological station (installed on the southern mouth of Barcelona harbour) were used to infer the predominant wind regime during the analysed upwelling episode that took place in late October – early November 2023. Complementarily, hourly snapshots of surface fields of temperature and chlorophyll provided by diverse satellite missions were extracted from the Copernicus Marine Service viewer[3] and used to analyse the impact of an intense upwelling event on their spatial distribution. Finally, a Copernicus satellite image map of cloud cover and hourly maps of sea level pressure and wind at 10 m height were employed to briefly characterize storm Babet.

[3] https://data.marine.copernicus.eu/viewer/expert

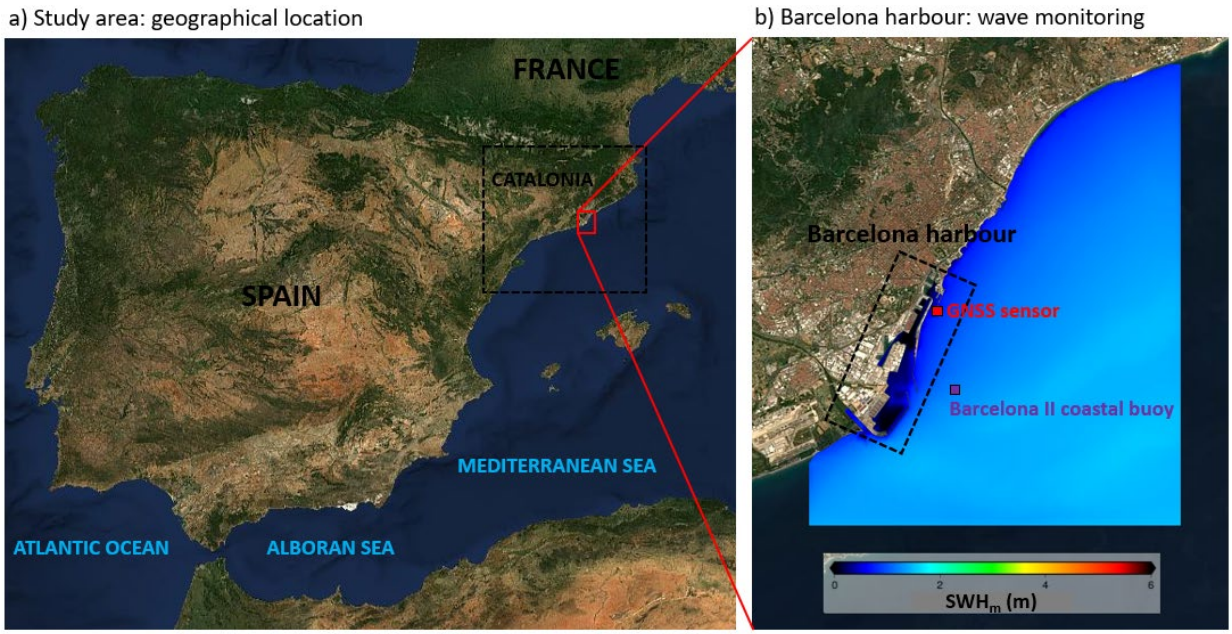

Figure 1. Wave model validation: a) Study area: Barcelona harbour, in the NW Mediterranean Sea; b) Harbour layout and wave monitoring: snapshot of the hourly significant wave height (SWHm) field predicted by the high-resolution coastal wave model for the 11th of December 2023 (00 h, local time). Red and purple squares indicate the location of a low-cost Global Navigation Satellite System (GNSS) sensor deployed in EuroSea, and Barcelona II coastal buoy, respectively. Barcelona harbour is marked with a dashed black rectangle.

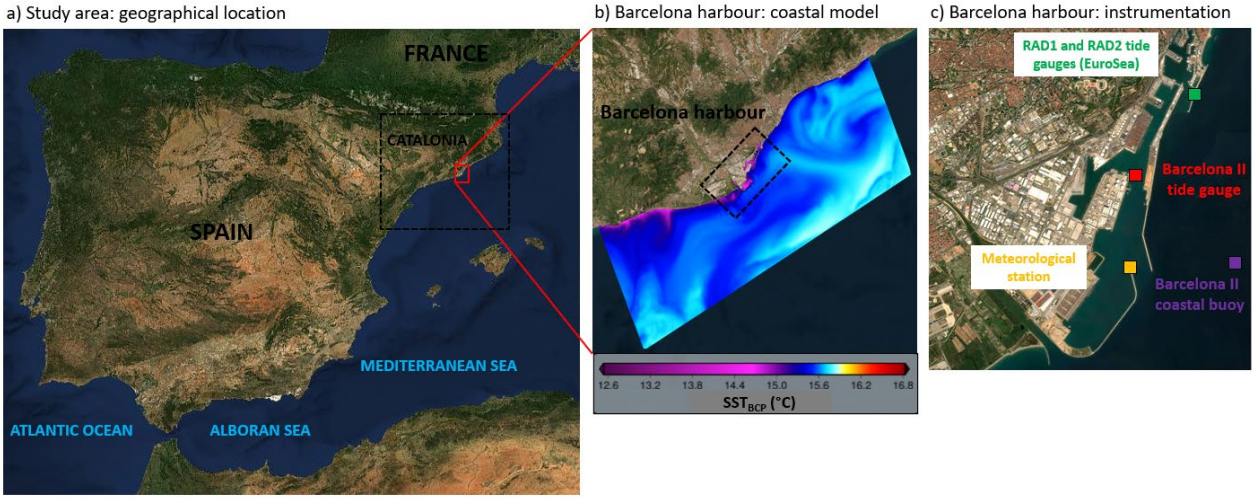

Figure 2. Circulation model validation: a) Study area: Barcelona harbour, in the NW Mediterranean Sea; b) snapshot of the hourly sea surface temperature (SST_{BCP}) field predicted by the high-resolution coastal (non-coupled) BCP model for the 15th of December 2023 (00 h, local time). Barcelona harbour is marked with a dashed black rectangle.; c) Harbour layout and met-ocean sensors monitoring: red and purple squares indicate the location of Barcelona II tide-gauge and Barcelona II coastal buoy, respectively. The green square denoted the location of two new radar tide-gauges deployed in the frame of EuroSea project. The orange square represents the location of a meteorological station.

2.2. Taranto pilot site

In June 2023 a solar-powered tide gauge was installed in the Port of Taranto (Figure 3) equipped with dual sea level sensors (1 conventional radar sensor, plus a MIROS wave monitoring radar sensor), a Global Navigation Satellite System (GNSS) receiver enabled for monitoring vertical land motion, plus sea level and

wave monitoring via Interferometric Reflectometry (GNSS-IR)), a barometer, data logging equipment, solar panels, a battery array and dual data telemetry systems. This system has low maintenance requirements and low running costs to ensure the longevity of the gauge. Sea level data from the radar sensor

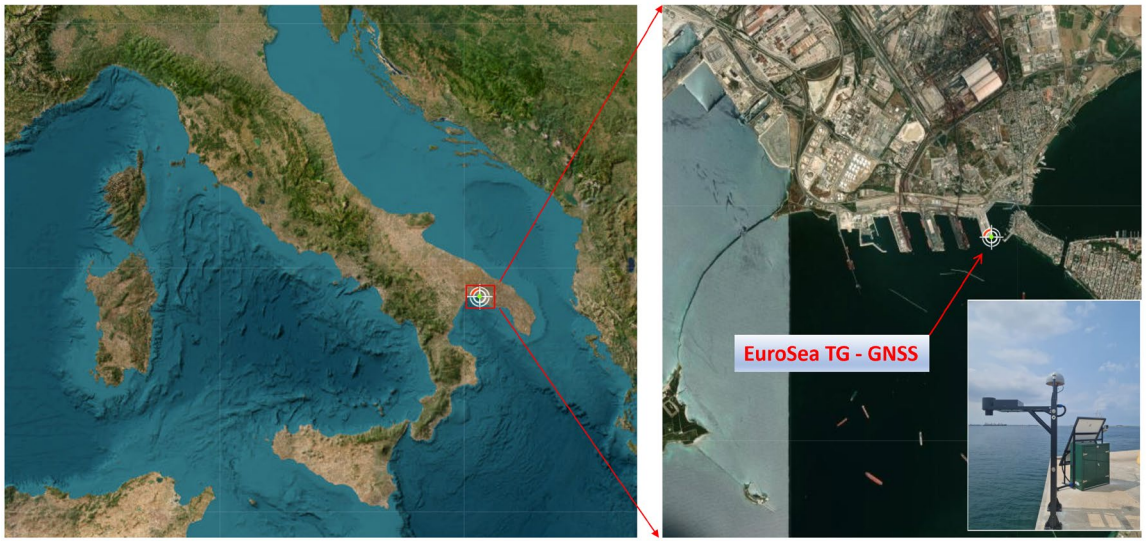

Figure 3. Study area of Taranto pilot site. Left: Taranto harbour in Southern Italy, in the Central Mediterranean Sea; b) Harbour layout and location of the new equipment deployed in EuroSea, tide gauge and GNSS.

3. Coastal Models Overview

An overview of the high-resolution coastal scale models implemented in OSPAC demonstrator is included in this section. More details can be found in *Deliverable 5.3: CMEMS downscaled circulation operational forecast system*[1] and *Deliverable 5.4*[2]*: CMEMS downscaled wave operational forecast system.*

3.1. Barcelona pilot site

The validation exercise for the circulation coastal models in Barcelona is based on the assessment of the two modelling systems currently operational in Puertos del Estado, and developed in the frame of EuroSea project by the team of Laboratorio de Ingeniería Marítima-Universidad Politécnica de Cataluña (LIM-UPC): one without waves-currents coupling (which will be referred here on as BCP) and another one, more recent, with waves-currents coupling (which will be referred here on as BCC). It is worth mentioning that BCP is referred to as OSPAC-V1, and BCC as OSPAC-V2, respectively, in Deliverable 5.3.

The LIM-UPC team has developed a high-resolution 3D hydrodynamic tool to comprehensively analyse the dynamics of local domains, in particular the coastal waters surrounding Barcelona harbour. This tool, described in detail in deliverables D5.3 and D5.4, uses the Coupled Ocean-Atmosphere-Wave-Sediment Transport (COAWST) Modelling System (Warner et al., 2010), coupling the SWAN (Simulating Waves Nearshore) wave model with the Regional Ocean Modelling System (ROMS) circulation model through the Model Coupling Toolkit (MCT), in BCC (OSPAC-V2) modelling system. This integration provides a comprehensive and dynamical framework required for understanding coastal dynamics and predicting interactions between wave and ocean circulation, especially in the Barcelona pilot case.

The COAWST Modelling System is an advanced computational tool for coastal, oceanic and atmospheric research. It integrates different models using the Model Coupling Toolkit (MCT) to facilitate dynamic environmental interactions.

The Model Coupling Toolkit (MCT)

The MCT is a powerful software library for coupling scientific models in computer simulations. MCT facilitates efficient and accurate data transfer between different models, allowing them to interact and exchange information in a synchronised manner (Jacob et al., 2005). It's essential for managing complex interactions in environmental modelling, particularly in systems such as COAWST that combine ocean and wave models.

MCT plays a critical role in COAWST, managing the exchange of data such as wind stress and temperature between models to ensure synchronised and efficient simulation processes. This toolkit enables the coupling of ROMS (Regional Ocean Modelling System) and SWAN (Simulating Waves Nearshore) models, improving the accuracy of coupled ocean-wave process simulations. In addition, MCT supports bidirectional grid refinement and improves simulation accuracy through precise variable field exchange.

Wave model

Barcelona wave forecasting system is composed of a variety of local-scale wave numerical models with 3-day ahead forecast horizon developed specifically for ports and their immediate environment. The system is based on SWAN wave model (Booij et al., 1999) and considers the transformations undergone by the waves as they approach the coast (the model accounts for wave-induced set-up). These model applications have high horizontal resolutions which range from 350 m to 150 m, depending on the size of the coastal area to be studied and the geographical complexities of the study area. In the case of Barcelona harbour, the spatial domain is shown in Figure 1b and the netcdf files are freely available[4].

The SWAN model, a key component of the COAWST Modelling System, has been carefully designed to simulate wave dynamics in coastal and nearshore regions. SWAN uses advanced numerical techniques to model wave generation, propagation and transformation, taking into account a range of physical processes. These include wind input, which drives wave formation, whitecapping (the breaking of wave crests in deep water), bottom friction (interaction with the seabed) and depth-induced breaking (waves breaking due to shallow depth).

At the Barcelona pilot site, the application of SWAN provides detailed insights into the spatial and temporal patterns of wave characteristics such as wave height, period and direction. This integrated approach is essential for accurate coastal management and decision-making, especially in complex coastal environments such as Barcelona.

Furthermore, the integration of SWAN into the COAWST framework facilitates a comprehensive understanding of the interaction between waves and other environmental components such as ocean currents and atmospheric conditions.

Circulation models

Barcelona coastal circulation system (BCP), based on ROMS model, is running operationally at EPPE since January 2022 (Figure 2b). ROMS is a three-dimensional, free-surface, topography-following numerical model that solves finite difference approximations of Reynolds Averaged Navier Stokes (RANS) equations using

[4] https://portuscopia.puertos.es/

hydrostatic and Boussinesq approximations with a split-explicit time-stepping algorithm (Shchepetkin and McWilliams, 2005 and 2009; Haidvogel et al., 2008). In addition, ROMS includes options for various model components such as different advection schemes (second, third, and fourth order), turbulence closure models (e.g., Generic Length Scale mixing, Mellor-Yamada, Brunt-Väisälä frequency mixing, user-provided analytical expressions, K-profile parameterization), and several options for boundary conditions.

Barcelona coastal coupled (wave-currents) system (BCC) is running pre-operationally at EPPE since late August 2023. While the ocean circulation simulations are based on ROMS Model (same as for BCP), wave simulations were based on SWAN. The simulations are based on a two-way coupling between ROMS and SWAN running on the same computational grid. Here it was used the latest available versions of the ROMS model (version 3.9) and the SWAN Model (version 41.31).

The ROMS within the Coupled Ocean-Atmosphere-Wave-Sediment Transport (COAWST) modelling system is a state-of-the-art, numerically robust tool for simulating ocean circulation (Shchepetkin and McWilliams, 2005; Haidvogel et al., 2008; Shchepetkin and McWilliams, 2009). As a 3D, free-surface, terrain-following, primitive equation model, ROMS is uniquely suited for high-resolution studies of coastal dynamics.

ROMS uses a split-explicit time-stepping scheme to accurately resolve fast surface gravity waves in tandem with slower hydrostatic and baroclinic motions. This feature is critical for maintaining computational efficiency while ensuring the accuracy of the simulation over a wide range of time scales. In addition, ROMS incorporates advanced vertical coordinate systems, such as S-coordinate, which optimise the representation of complex topographies and stratification patterns.

In addition, the integration of ROMS with other components of COAWST, such as the SWAN wave model, enhances the ability to study the complex interactions between ocean circulation, wave dynamics and atmospheric conditions.

For the Barcelona pilot site, ROMS is essential to capture the detailed ocean circulation patterns, thermal stratification and salinity variations. This includes the ability to simulate sub-mesoscale processes and coastal upwelling events, which are crucial for understanding the response of the local marine environment to both natural variability and anthropogenic forcing.

In summary, the COAWST Modelling System, through the integration of SWAN and ROMS models via the MCT, provides a comprehensive framework for studying and predicting the complex interactions between waves and ocean circulation. This approach is vital for in-depth analysis of coastal dynamics, supporting maritime planning and addressing environmental challenges, particularly within the Barcelona pilot site.

3.2. Taranto pilot site

CMCC developed an integrated very high-resolution modelling framework based on unstructured-grid approach for 3D hydrodynamic and waves. The modelling framework is able to investigate in past and short-term forecasting mode the coastal and port coastal water dynamics of Taranto. The modelling tool, described in detail into deliverables D5.3 and D5.4, uses the two state-of-art models which are SHYFEM for the hydrodynamics and WW3 for the waves. The interaction between the two models is done via an external coupler which includes radiation stress and surface drag coefficient from waves to ocean, and currents and sea level from ocean to waves. The two models run over the same unstructured grid, with variable resolution from 3km in open ocean to 100m overall the coastal waters of the Taranto Gulf and 20m in the Taranto Seas and surrounding areas.

Wave model

The model is WAVEWATCH III™, a community wave modelling framework that includes the latest scientific advancements in the field of wind-wave modelling and dynamics. The core of the framework consists of the WAVEWATCH III third-generation wave model, developed at the US National Centers for Environmental Prediction (NOAA/NCEP) in the spirit of the WAM model (Komen et al., 1984).

WAVEWATCH III, hereafter WW3 solves the random phase spectral action density balance equation for wavenumber-direction spectra. The implicit assumption of this equation is that properties of medium (water depth and current) as well as the wave field itself vary on time and space scales that are much larger than the variation scales of a single wave. The model includes options for shallow-water (surf zone) applications, as well as wetting and drying of grid points. Propagation of a wave spectrum is solved on unstructured (triangular) grid for the Taranto implementation. Source terms for physical processes include parameterizations for wave growth due to the actions of wind, exact and parametrized forms accounting for nonlinear resonant wave-wave interactions, scattering due to wave-bottom interactions, triad interactions, and dissipation due to whitecapping, bottom friction, surf-breaking, and interactions with mud and ice. The model includes several alleviation methods for the Garden Sprinkler Effect, and computes other transformation processes such as the effects of surface currents to wind and wave fields, and sub-grid blocking due to unresolved islands.

The modelling approach is based on the downscaling of CMEMS Marine products released at the regional scale of Mediterranean Sea. The current Med_Waves-CMEMS (Korres et al., 2021) implementation is based on WAM Cycle 4.6.2 with proper tuning and maximum spectral steepness limitation and it has been developed as a nested sequence of two computational grids (coarse and fine) to ensure that swell propagating from the North Atlantic (NA) towards the strait of Gibraltar is correctly entering the Mediterranean Sea (MED). The Med-Waves model solutions are corrected by an optimal interpolation data assimilation scheme of along-track significant satellite wave height observations.

Detailed description of model physics and numerics, set-up, parametrization and forcings could be found in Deliverable 5.4[2].

Circulation model

The circulation model is SHYFEM model, which is a 3-D finite element hydrodynamic model (Umgiesser et al., 2004 and 2014, Micaletto et al., 2022) solving the Navier–Stokes equations by applying hydrostatic and Boussinesq approximations. The unstructured grid is Arakawa B with triangular meshes (Bellafiore and Umgiesser, 2010; Ferrarin et al., 2013), which provides an accurate description of irregular coastal boundaries. The model uses a semi-implicit algorithm for integration over time, which has the advantage of being unconditionally stable with respect to gravity waves, bottom friction and Coriolis terms, and allows transport variables to be solved explicitly. The Coriolis term and pressure gradient in the momentum equation, and the divergence terms in the continuity equation are treated semi-implicitly. Bottom friction and vertical eddy viscosity are treated fully implicitly for stability reasons, while the remaining terms (advective and horizontal diffusion terms in the momentum equation) are treated explicitly. The modelling approach is based on the downscaling of CMEMS Marine products released at the regional scale of Mediterranean Sea. The current Med-CMEMS implementation is based on NEMO (Nucleus for European Modelling of the Ocean; Madec, 2008) finite-difference code with a horizontal resolution of 1/24 of a degree (4–5 km approximately) and 141 unevenly spaced vertical levels. The system is provided by a data assimilation system based on the 3D-VAR scheme developed by Dobricic and Pinardi (2008). Detailed

description of model physics and numerics, set-up, parametrization and forcings could be found in Deliverable 5.3.

4. Validation Methodology

4.1. Barcelona pilot site

Previous context: validation during model implementation

The validation methodology for the Barcelona Pilot site within the EuroSea project was carefully designed to be replicable, ensuring the effectiveness of the approach (described in detail into Deliverables D5.3[1] and D5.4[2]). It includes:

- Model Implementation and Configuration: Using the COAWST modelling system, integrating ROMS and SWAN models, nested within CMEMS-IBI products, driven by high-frequency sea surface data.
- Coupling and Data Exchange: Two-way ocean refinement and one-way wave refinement enable full coupling between the models, facilitating key parameter exchanges.
- Nested Grid System: A two-nested grid configuration enhances spatial resolution, allowing for detailed analyses of coastal and port areas.
- Validation with Field Campaign Data: The methodology's effectiveness was validated through a field campaign by the LIM-UPC work team between March and April 2022. During this period, the severe CELIA storm and other significant storms were monitored, generating high wave heights. These real-world data sets were then compared with the outputs from our coupled wave-current model. The comparison revealed a strong correlation between the modelled results and the in-situ observations, underscoring the reliability and accuracy of our methodology. These validation results are comprehensively detailed in Deliverable 5.4.

This comprehensive methodology establishes a robust framework for accurate and reliable oceanographic modelling at the Barcelona Pilot site, part of the EuroSea project.

The integration of advanced models, coupled with high-resolution data and innovative grid systems, exemplifies a state-of-the-art approach in marine forecasting. This process not only validates the current project but also sets a precedent for future oceanographic research and operational forecasting, underscoring the project's commitment to advancing marine science.

Wave model validation

The accuracy of the high-resolution coastal wave model was evaluated at those two grid points closest to the observational data sources. In particular, we selected:

i) the model grid point (2.190°E-41.361°N) closest to the GNSS sensor (2.185°E-41.358°N), which is located at a distance of 530 m.

ii) the model grid point (2.200°E-41.319°N) closest to Barcelona II coastal buoy (2.200°E-41.320°N), which is located at a distance of 90 m.

In the case of the GNSS sensor, concurrent estimations of hourly SWH_o and SWH_m were compared for the 6-month period June-November 2023. Histograms, quantile-quantile (QQ) plot and the best linear fit of scatter plot were also computed. The statistical metrics used in the present study to compare two data sets included the mean, the standard deviation, and the Pearson correlation coefficient (Emery and Thompson, 2001). In

the case of Barcelona II coastal buoy, not only concurrent estimations of hourly SWH_o and SWH_m were compared but also estimations of Tm and wave incoming direction were compared both qualitatively and quantitatively.

Finally, it is worth mentioning that only hindcast (or best estimate) outcomes from the wave model were used, while longer forecast horizons were not analysed. Table 1 displays both observational and model data sources used for the wave model validation exercise in Barcelona.

Table 1. Wave data sources used in this study. GNSS, SWH_o, SWH_m, T_{mo}, T_{mm}, MWD_o and MWD_m stand for Global Navigation Satellite System, observed significant wave height, modelled significant wave height, observed mean wave period, modelled mean wave period, observed mean incoming wave direction and modelled mean incoming wave direction, respectively.

Source	Type	Location (coverage)	Variable (unit)	Temporal resolution	Time span used	Spatial resolution
In situ sensor	Barcelona II Buoy	Coastal location (2.20°E – 41.32°N)	SWH_o (m)	Hourly	June-November 2023	Point-wise location
			T_{mo} (s)			
			MWD_o (°)			
In situ sensor	GNSS sensor	Port location (2.185°W – 41.358°N)	SWH_o (m)	Hourly	June-November 2023	Point-wise location
Numerical Model	Wave forecast system	Coastal domain (2.1°E – 2.5°E 41.25°N – 47.50°N)	SWH_m (m)	Hourly	June-November 2023	0.0034°
			T_{mm} (s)			
			MWD_m (°)			

Circulation model validation

The accuracy of both high-resolution coastal circulation models was evaluated at those three grid points closest to the observational data sources. In particular, we selected:

iii) the model grid point (2.198°E-41.319°N) closest to Barcelona II coastal buoy (2.200°E-41.320°N), which is located at a distance of 200 m.

iv) the model grid point (2.181°E-41.339°N) closest to Barcelona II tide gauge (2.170°E – 41.340°N), which is located at a distance of 930 m.

v) the model grid point (2.192°E-41.352°N) closest to RAD1 and RAD 2 tide gauges (2.190°E – 41.360°N), which is located at a distance of 910 m.

In the case of Barcelona II coastal buoy, concurrent estimations of hourly SST_o, SST_{BCP} and SST_{BCC} were compared for the 3-month period September-November 2023. In the case of the three tide gauges employed

in the present study, concurrent estimations of hourly SSH_o, SSH_{BCP} and SSH_{BCC} were compared for the selected period. Timeseries were visually compared and the best linear fit of scatter plot was also computed. The statistical metrics used in the present study to compare two data sets included the mean, the standard deviation, the root mean squared error (RMSE) and the Pearson correlation coefficient (Emery and Thompson, 2001). It is worth mentioning that different forecast horizons were analysed in order to quantify the loss of precision for longer horizons. To this end, the hindcast (or best estimate, named HC01 hereinafter) was compared against the +24 h forecast (FC01), +48 h forecast (FC02) and +72 h forecast (FC03).

Finally, a brief qualitative analysis of an intense coastal upwelling event during late October – early November 2023 was conducted in order to gain further insight into both coastal models' ability to adequately represent this type of well-documented phenomenon in terms of the associated surface current patterns. Table 2 summarizes both observational and model data sources used for the circulation model validation exercise in Barcelona.

Table 2. Circulation data sources used in this study for validation purposes. SST_o and SSH_o stand for observed sea surface temperature and sea surface height, respectively. SST_{BCP} and SSH_{BCP} stand for sea surface temperature and sea surface height modelled by BCP non-coupled model, respectively. SST_{BCC} and SSH_{BCC} stand for sea surface temperature and sea surface height modelled by BCC coupled model, respectively.

Source	Type	Location (coverage)	Variable (unit)	Temporal resolution	Time span used	Spatial resolution
In situ sensor	Barcelona II Buoy	Coastal location (2.20°E – 41.32°N)	SST_o (°C)	Hourly	September-November 2023	Point-wise location
In situ sensor	Barcelona II tide gauge	Port location (2.17°E – 41.34°N)	SSH_o (m)	Hourly	September-November 2023	Point-wise location
In situ sensor	RAD1 tide gauge	Port location (2.19°E – 41.36°N)	SSH_o (m)	Hourly	September-November 2023	Point-wise location
In situ sensor	RAD II tide gauge	Port location (2.19°E – 41.36°N)	SSH_o (m)	Hourly	September-November 2023	Point-wise location
BCP ocean model	Non-coupled forecast system	Coastal domain (1.80°E – 2.54°E 41.01°N – 41.55°N)	SST_{BCP} (°C)	Hourly	September-November 2023	0.00328°
			SSH_{BCP} (m)			
BCC ocean Model	Coupled forecast system	Coastal domain (1.80°E – 2.54°E 41.01°N – 41.55°N)	SST_{BCC} (°C)	Hourly	September-November 2023	0.00328°
			SSH_{BCC} (m)			

4.2. Taranto pilot site

The full validation of the models in simulation model for past events were reported in D5.3. and D5.4. Here we verify the effectiveness of the modelling against the new data installed in Taranto (described in section 2.2.) for the period ranging from September 2023 (installation) to the end of November 2023. Timeseries of significant wave height and sea level with BIAS and RMSE are used for the metrics.

5. Validation Results

5.1. Barcelona pilot site

The Port of Barcelona is a major port in Barcelona, Catalonia, NE Spain (Figure 1 and Figure 2). This 7.86 km^2 port is managed by the Port Authority of Barcelona, itself owned by the state-owned Ports of the State. It is not only the cruiser port with most passengers in the Mediterranean but also the third largest container port in the country and the ninth largest in Europe, with a trade volume of 3.42 million TEUs in 2018.

From an oceanographic perspective, the predominant circulation in the Catalonian continental margin is characterized by the presence of the quasi-permanent barotropic shelf-slope jet which flows along-shore south-westward. This current, called Liguro-Provenzal-Catalan current or simply 'the North Current', is in geostrophic balance with the so-called Catalan front, which is a permanent density front associated to strong salinity gradients. The quasi-permanent SW flow is only altered by clockwise inertial oscillations (with maximum occurrence during the warm stratified season) and some short periods of current reversals, related to mesoscale events like frontal instabilities, meanders, eddies and filaments (Grifoll et al., 2015). The intensity of mean currents is relatively low (10-20 $cm \cdot s^{-1}$) and increases in autumn as a result of both the intensification of the mesoscale activity and the local wind variability. Furthermore, the Catalonian coast is characterized by a wave regime where the mean wave period is usually low (Sánchez-Arcilla et al., 2008). Strong north-westerly winds typically induce waves that propagate offshore, although waves from the east and the south are also significant.

Wave model validation

Comparison of wave estimations provided by the GNSS sensor

In this section, a model skill assessment was conducted in order to infer the accuracy of the coastal wave model to adequately reproduce SWH estimations in port-approach areas (denoted in Figure 1b). To this aim, we selected the model grid point closest to the GNSS station (530 m far away), which was installed at the northern entrance of the harbour.

There was a noticeable similarity among the coastal model and Barcelona II buoy hourly timeseries for the selected 6-month period, despite the relevant gaps in the GNSS data provision, with only a 37% of available concurrent data (4a) due to a power failure. The most prominent peaks, which lied in the range 1.5–2.5 m, were fairly well captured by the model.

The histogram for each dataset (4b), showing the number of hourly wave height estimations per class interval, exhibited a Rayleigh-like distribution clustered around 0.4 m mean and shifted to lower values. Both

datasets show similar positive skew and variability, with the standard deviation emerging around 0.27 m for the analysed period.

Based on the QQ plot (4c), it can be concluded that wave height modelled estimations were consistent despite the slight underestimation (overestimation) detected for low (high) sea states. Furthermore, the results derived from the best linear fit of scatter plot (Figure 4d) showed that the slope was close to 1 and the related Pearson correlation coefficient was significantly high (0.87).

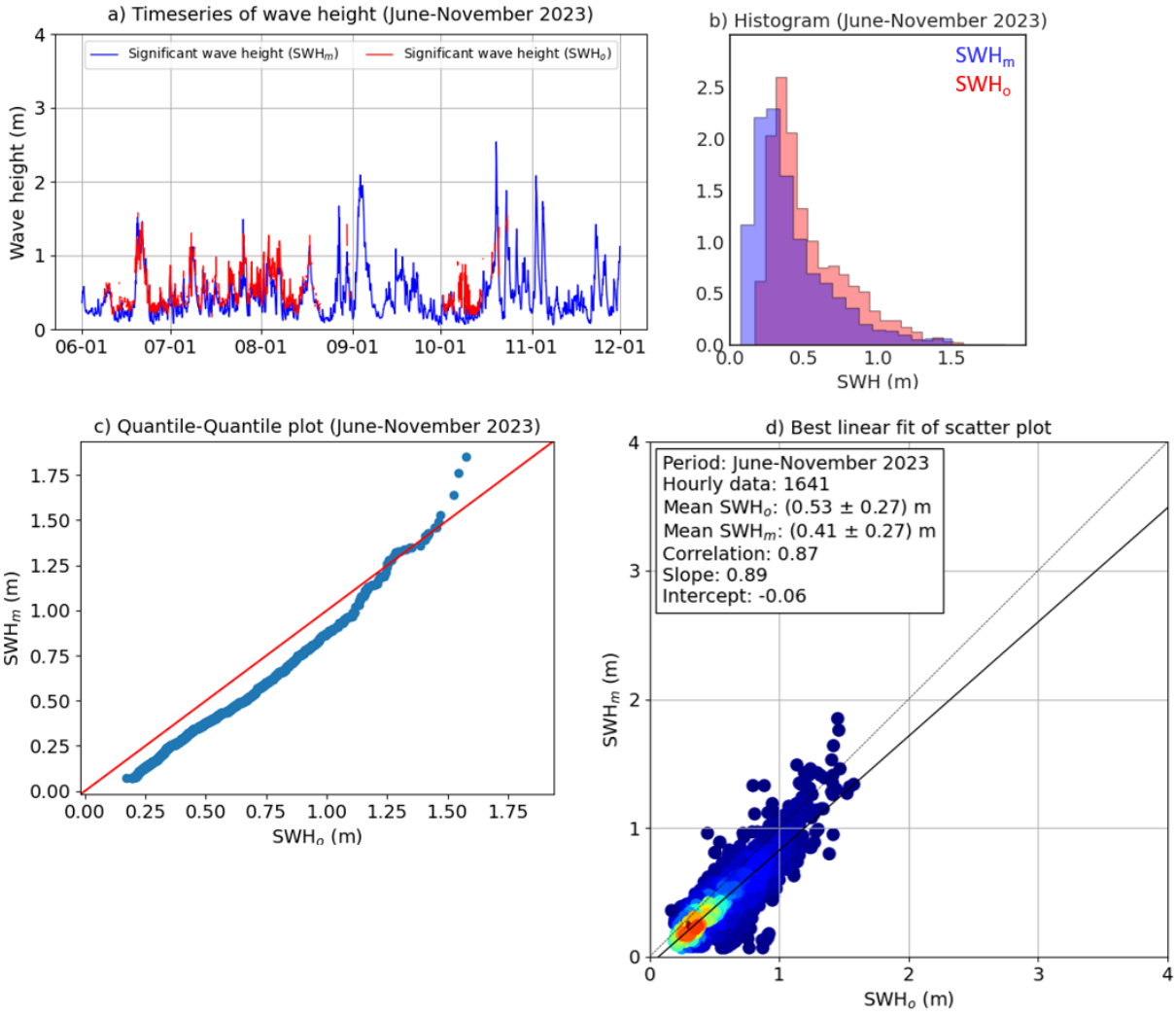

Figure 4. Skill assessment of the high-resolution coastal wave model at the grid point closest to the GNSS station installed in Barcelona harbour for a 6-month period (June-November 2023): a) hourly timeseries of significant wave heigh modelled (SWH$_m$, blue line) and observed (SWH$_o$, red line) by the GNSS sensor; b) histogram of concurrent hourly estimations of SWH$_m$ (blue bins) and SWH$_o$ (red bins); c) Quantile-quantile (QQ) plot of SWH for the 6-month period analysed; d) best linear fit (solid black line) of scatter plot between hourly estimations of SWH$_m$ and SWH$_o$. The dotted black line represents the result of perfect agreement with slope 1.0 and intercept 0. Statistical metrics are adhered in white box (upper left corner).

Comparison of wave estimations provided by Barcelona II coastal buoy

In this section, a multi-parameters skill assessment was performed in order to infer the accuracy of the wave model to adequately reproduce SWH estimations in coastal areas. To this aim, we selected the model grid

point closest to Barcelona II moored buoy (90 m far away) and compared the hourly timeseries (5a). It is worth mentioning the almost seamless in situ wave data provision (99.11%), which highlights the consistent performance of Barcelona II coastal buoy during the analysed period. The resemblance between both timeseries is extremely high, especially for wave height values below 1.5 m. The most prominent peaks, which lied in the range 2–3.8 m, were fairly well captured by the model and even overestimated during September and October. The histograms, computed for each dataset (5b), exhibited again a Rayleigh-like distribution clustered around 0.4 m mean and shifted to lower values. Both datasets show similar positive skew and variability, with the standard deviation emerging in the range 0.43-0.48 m for the analysed period. Based on the QQ plot (5c), we can infer that wave height model outputs were very precise for wave heights ranging from 0.2 m to 1.5 m, whereas a slight overestimation was detected for higher sea states. Furthermore, the results derived from the best linear fit of scatter plot (Figure 4d) showed that the slope was very close to 1 and the related Pearson correlation coefficient was significantly high (0.95).

With regards to the mean wave period, there was a noticeable visual resemblance between the model and Barcelona II coastal buoy hourly timeseries for the selected 6-month period (6a). The histogram of mean wave period estimations per class interval revealed a rather symmetrical (almost Gaussian-like) distribution, centred around 3.5 s and slightly shifted to lower values (Figure 5b). According to the QQ plot (Figure 5c), there was a slight underestimation of the lower wave periods (below 3 s), whereas a moderate overestimation for higher periods (above 5 s) was observed. The best linear fit of scatter plot exhibited relevant skill metrics: the slope was close to 1 and the associated Pearson correlation coefficient was significantly high (0.86).

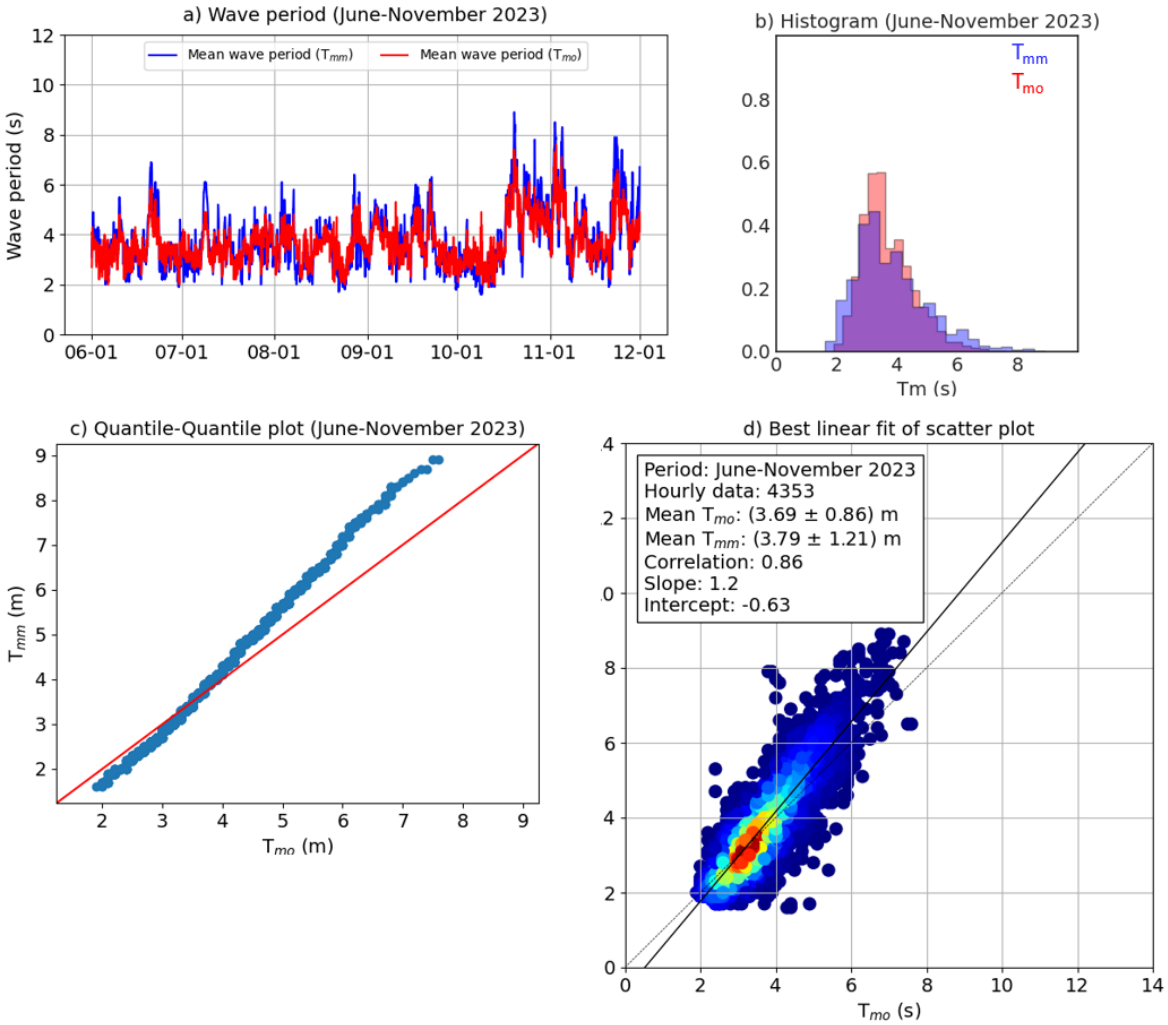

Figure 5. Skill assessment of the high-resolution coastal wave model at the grid point closest to Barcelona II coastal buoy for a 6-month period (June-November 2023): a) hourly timeseries of mean wave period modelled (T_{mm}, blue line) and observed (T_{mo}, red line) by the coastal buoy; b) histogram of concurrent hourly estimations of T_{mm} (blue bins) and T_{mo} (red bins); c) Quantile-quantile (QQ) plot of T_m for the 6-month period analysed; d) best linear fit (solid black line) of scatter plot between hourly estimations of T_{mm} and T_{mo}. The dotted black line represents the result of perfect agreement with slope 1.0 and intercept 0. Statistical metrics are adhered in white box (upper left corner).

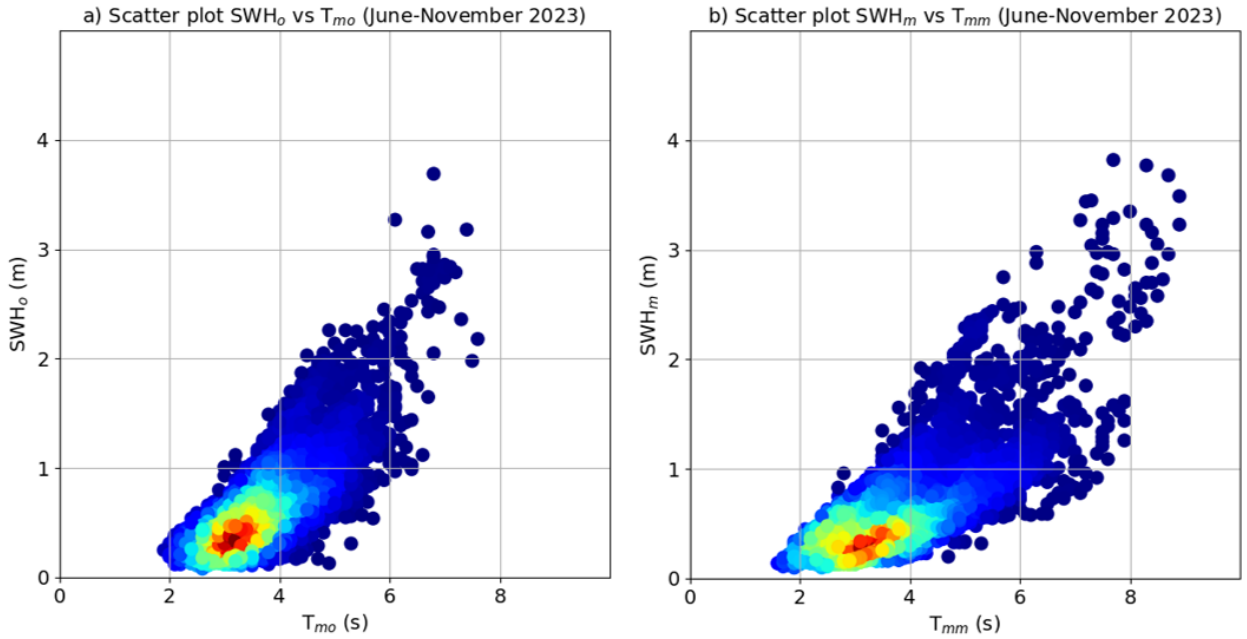

Figure 6. a) Scatter plots of observed significant wave height (SWH_o) and mean wave period (T_{mo}) estimations provided by Barcelona II coastal buoy for a 6-month period (June-November 2023); b) Scatter plots of modelled significant wave height (SWH_m) and mean wave period (T_{mm}) estimations provided by the coastal wave model at the grid point closest to Barcelona II coastal buoy.

The most common wave conditions in Barcelona coastal areas during the analysed period were qualitatively characterized by determining the ranges of wave heights and periods that represent the majority of sea states (Figure 6). The scatter plots relating the significant wave height and period were computed for both in situ estimations provided by Barcelona II coastal buoy (Figure 6a) and model outcomes (Figure 6b). Some similarities were observed between the scatter plots, despite the higher dispersion of model estimations. In addition, a linear relationship between both parameters was evidenced: the highest wave height events (above 3 m) also presented the longest wave periods: 6–7.7 s and 6–9 s for the coastal buoy and model estimations, respectively. Conversely, low sea-states (below 0.5 m) are associated with the shortest wave periods (below 6 s). Based on the density distributions, it can be stated that the most usual wave events in the vicinity of Barcelona harbour during June-November 2023 were defined by wave heights and periods in the ranges 0.2–0.8 m and 2–4 s, respectively.

In terms of mean incoming wave direction (Figure 7), the concordance between the wave roses derived from Barcelona II coastal buoy estimations (Figure 7a) and from the wave model outcomes (Figure 6b) for the 6-month period analysed was noticeable, with SW-S as the predominant sector and residual waves coming from the S, SE and E directions. Such spatial distribution appears to be clearly influenced by the Catalonian coastline morphology.

The analysis also revealed that high wave height events (above 2 m) usually were induced, most of the times, by south-westerly winds. The skill metrics confirmed the consistency of the coastal model performance, with a Pearson correlation coefficient of 0.79 (Figure 7c).

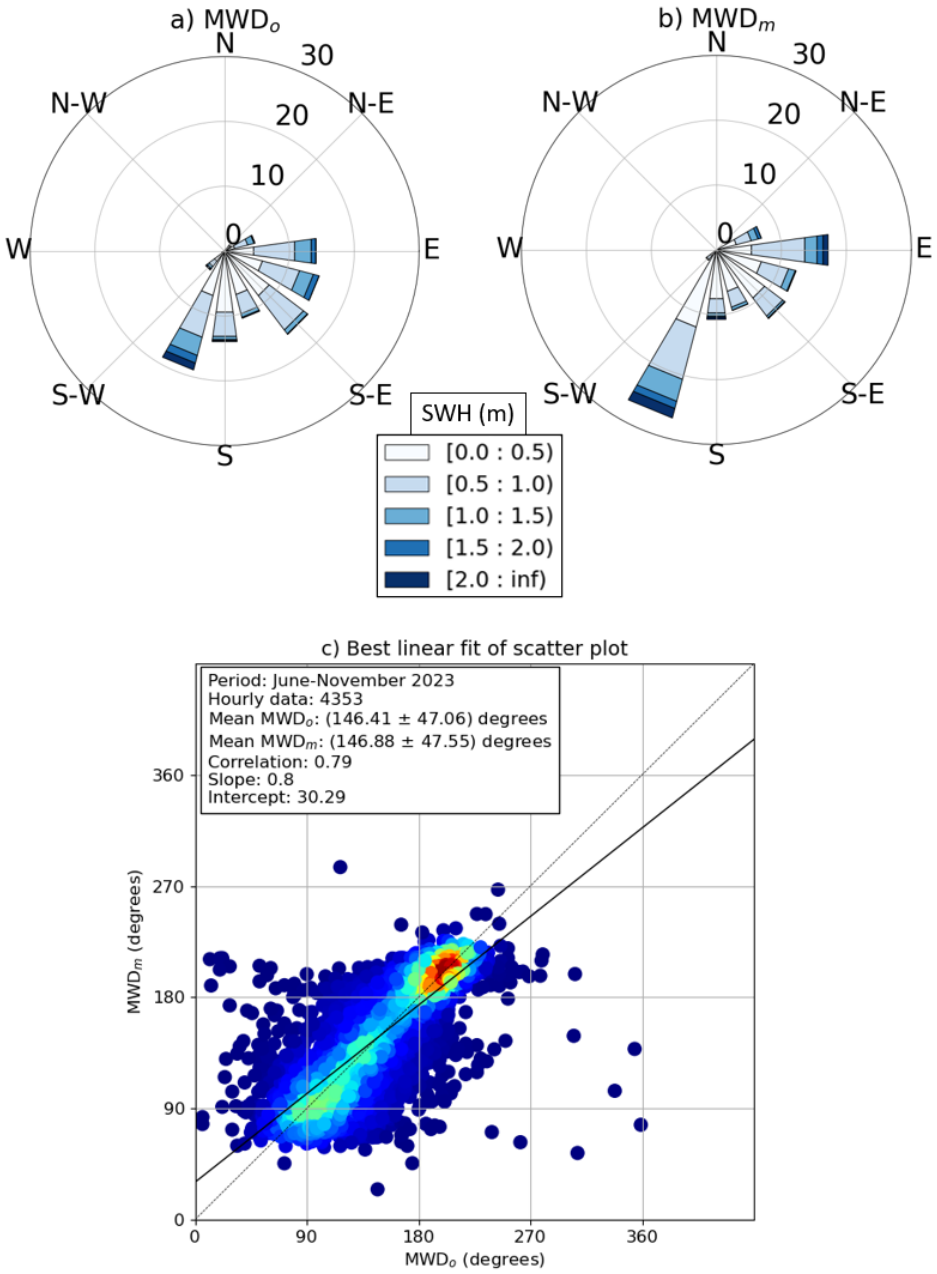

Figure 7. Comparison of the mean incoming wave directions for the 6-month period (June-November 2023): a) observed (MWD_o) at Barcelona II coastal buoy; b) modelled (MWD_m) at the grid point closest to the coastal buoy; c) best linear fit (solid black line) of scatter plot between hourly estimations of MWD_{mm} and MWD_{mo}. The dotted black line represents the result of perfect agreement with slope 1.0 and intercept 0. Statistical metrics are adhered in white box (upper left corner).

Circulation model validation

Model Inter-comparison of sea surface temperature

In this section, a model skill assessment was conducted in order to infer the accuracy of both coastal circulation models to adequately reproduce SST in situ observations. To this aim, we selected the model grid point closest to Barcelona II coastal buoy (200 m far away).

According to the hourly timeseries comparison, we can firstly state that the in-situ data provision during the selected period was almost complete (about 99.3%). Furthermore, there was a noticeable models-observation similarity for the selected 3-month period, regardless of the forecast horizon used: hindcast (HC01, shown in Figure 8a), +24 h forecast (FC01, Figure 9a), +48 h forecast (FC02, Figure 10a) and +72 h forecast (FC03, Figure 11a). In any case, models were able to qualitatively capture the 9°C drop (from 25°C to 16°C) of water temperature that took place during late October and early November 2023 as a consequence of an intense and long-lasting coastal upwelling episode that will be further described in section 4.4. Likewise, both models were also capable to reproduce the subsequent temperature increase (2°C) once the south-westerly winds that drove the upwelling event weakened and changed the predominant incoming direction. It is also interesting to point out the ability of BCC model to properly capture the sharp, sudden drop from 24°C to 20°C that took place around the 20th of October (marked with an orange ellipse in Figure 8a), whereas BCP was not able to reproduce such an intense cooling.

In terms of best linear fit of scatter plots (shown in Figure 8 b-c, Figure 9 b-c, Figure 10 b-c and Figure 11 b-c), the slope was moderately close to 1 and the related Pearson correlation coefficient was significantly high (above 0.96). The RMSE lied in the range [1.18-1.36] °C, with both models overestimating the SST values, especially during the upwelling event and the afterwards temperature heating.

The skill metrics were gathered in Table 3, revealing the following:

The models´ performances were comparable. BCP slightly outperformed BCC in terms of lower RMSE, higher correlations coefficients and slope values closer to 1.

A gradual loss of precision is observed in both models for longer forecast horizons, which is slight in the case of BCC (from 1.20°C to 1.36°C) and very slight in the case of BCP (from 1.18°C to 1.22°C).

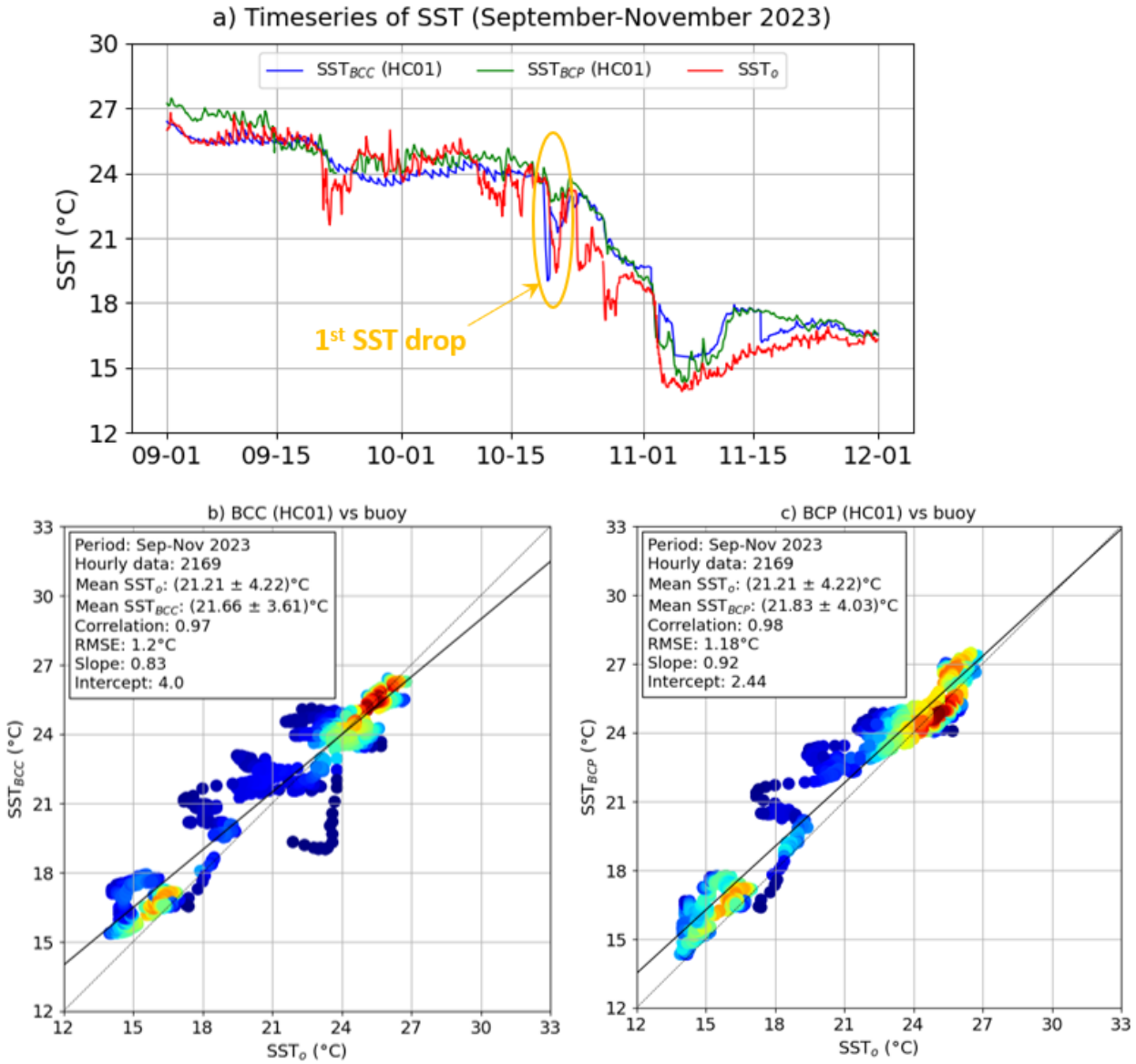

Figure 3. a) Models intercomparison against in situ estimations provided by Barcelona II coastal buoy for a 3-month period (September-November 2023): hourly timeseries of sea surface temperature from coupled BCC model (SST_{BCC}, green line), non-coupled BCP model (SST_{BCP}, blue line) and in situ observations (SST_o, red line); b) best linear fit (solid black line) of scatter plot between hourly estimations of SST_{BCC} and SST_o; c) best linear fit (solid black line) of scatter plot between hourly estimations of SST_{BCP} and SST_o. The dotted black line represents the result of perfect agreement with slope 1.0 and intercept 0. Statistical metrics are adhered in white box (upper left corner). In this example, hindcast or best estimates were used (HC01).

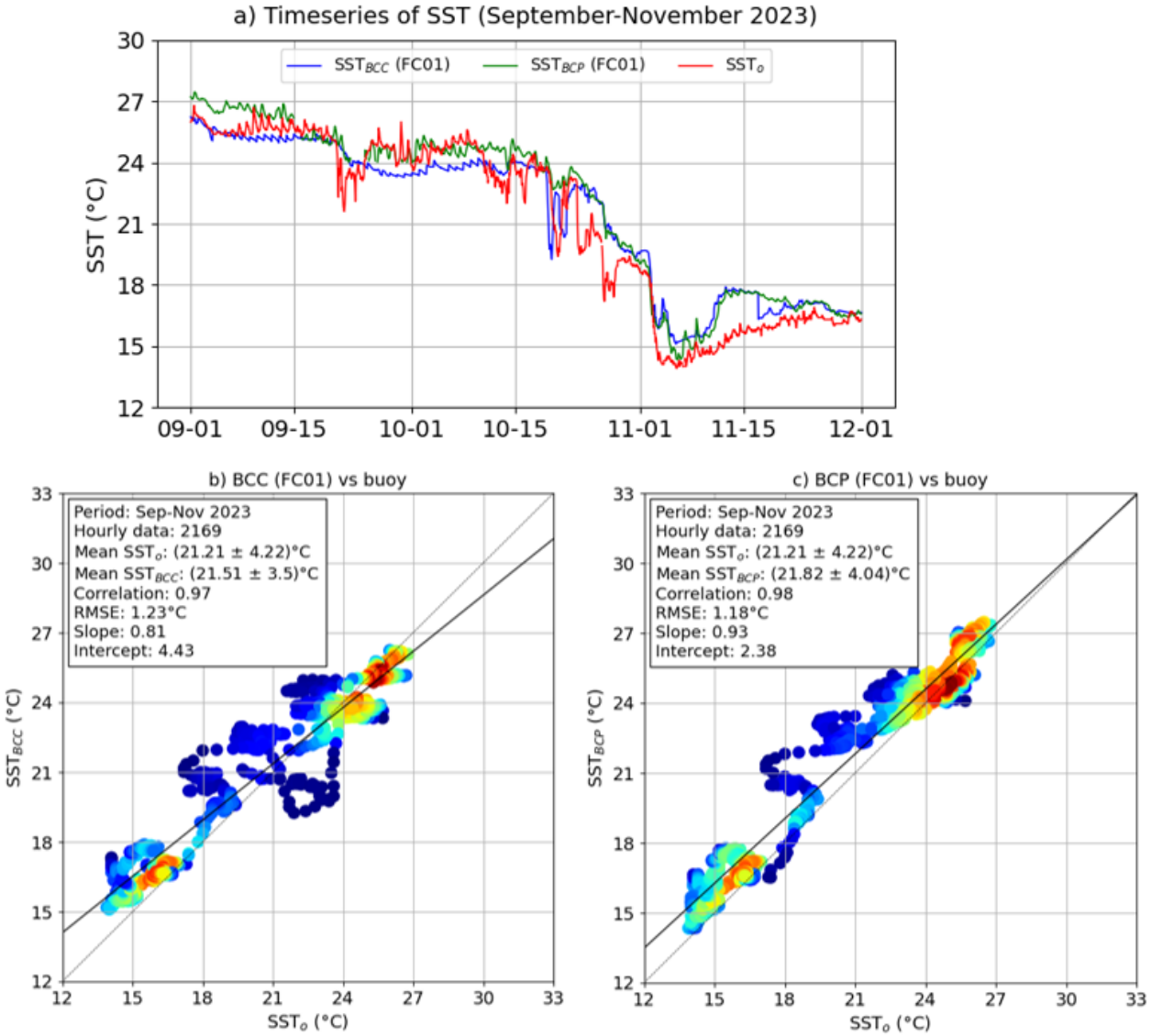

Figure 4. a) Models intercomparison against in situ estimations provided by Barcelona II coastal buoy for a 3-month period (September-November 2023): hourly timeseries of sea surface temperature from coupled BCC model (SST_{BCC}, green line), non-coupled BCP model (SST_{BCP}, blue line) and in situ observations (SST_o,, red line); b) best linear fit (solid black line) of scatter plot between hourly estimations of SST_{BCC} and SST_o; c) best linear fit (solid black line) of scatter plot between hourly estimations of SST_{BCP} and SST_o. The dotted black line represents the result of perfect agreement with slope 1.0 and intercept 0. Statistical metrics are adhered in white box (upper left corner). In this example, the +24 h forecast horizon was used (FC01).

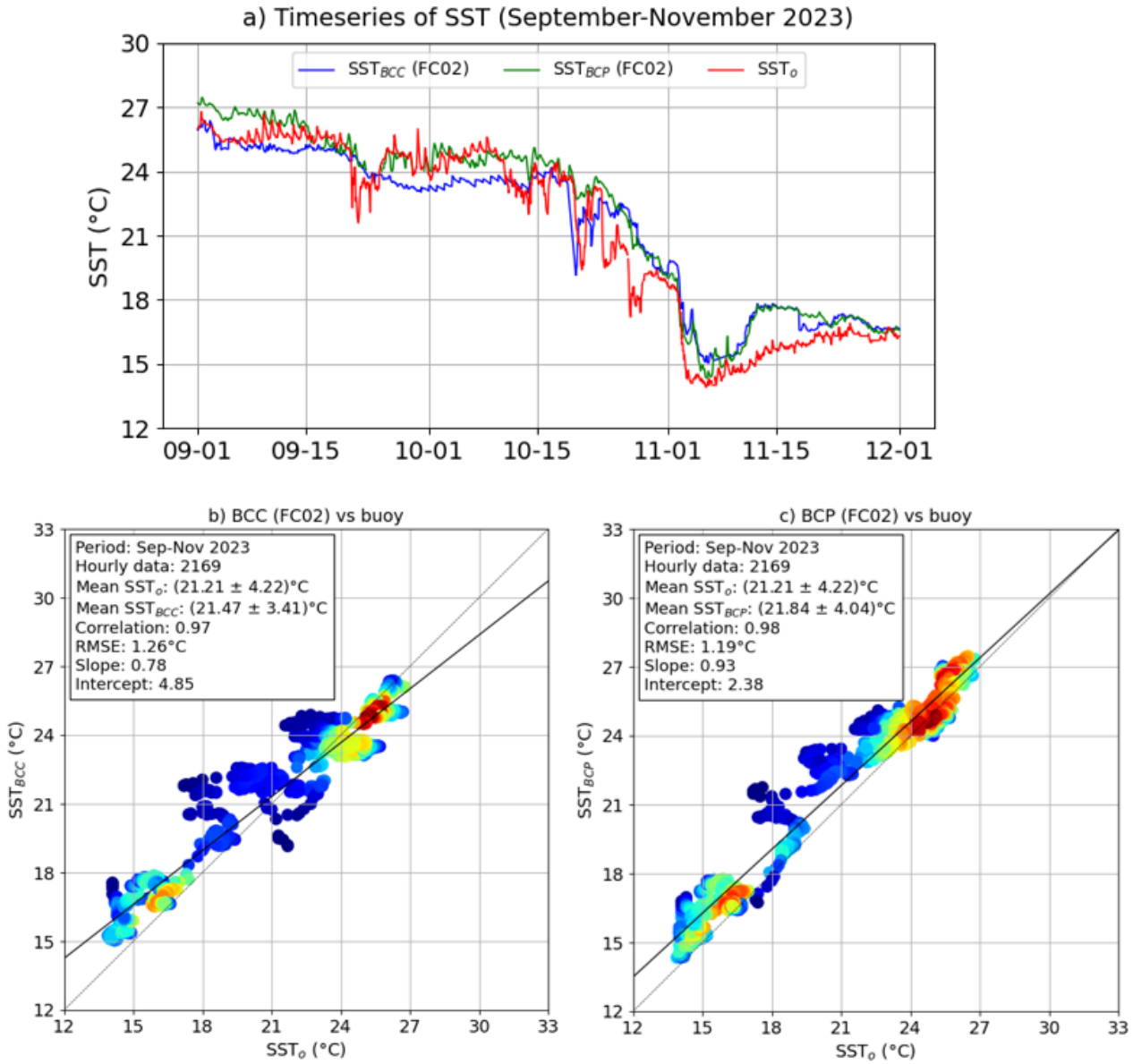

Figure 5. a) Models intercomparison against in situ estimations provided by Barcelona II coastal buoy for a 3-month period (September-November 2023): hourly timeseries of sea surface temperature from coupled BCC model (SST_{BCC}, green line), non-coupled BCP model (SST_{BCP}, blue line) and in situ observations (SST_o, red line); b) best linear fit (solid black line) of scatter plot between hourly estimations of SST_{BCC} and SST_o; c) best linear fit (solid black line) of scatter plot between hourly estimations of SST_{BCP} and SST_o. The dotted black line represents the result of perfect agreement with slope 1.0 and intercept 0. Statistical metrics are adhered in white box (upper left corner). In this example, the +48 h forecast horizon was used (FC02).

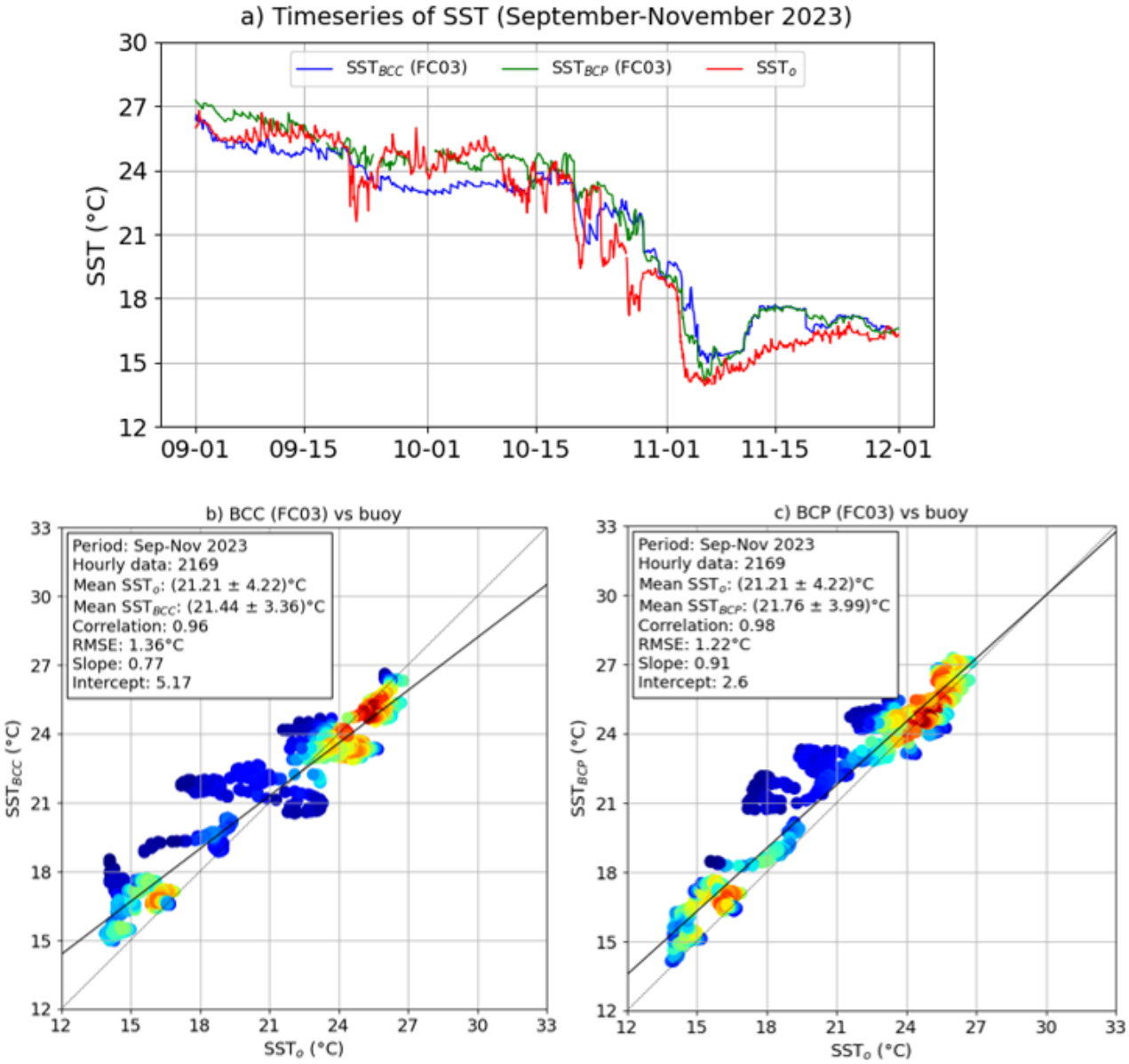

Figure 6. a) Models intercomparison against in situ estimations provided by Barcelona II coastal buoy for a 3-month period (September-November 2023): hourly timeseries of sea surface temperature from coupled BCC model (SST_{BCC}, green line), non-coupled BCP model (SST_{BCP}, blue line) and in situ observations (SST_o,, red line); b) best linear fit (solid black line) of scatter plot between hourly estimations of SST_{BCC} and SST_o; c) best linear fit (solid black line) of scatter plot between hourly estimations of SST_{BCP} and SST_o. The dotted black line represents the result of perfect agreement with slope 1.0 and intercept 0. Statistical metrics are adhered in white box (upper left corner). In this example, the +72 h forecast horizon was used (FC03).

Table 3. Summary of metrics derived from the models intercomparison of sea surface temperature (SST) against in situ estimations provided by Barcelona II coastal buoy for the 3-month period September-November 2023. The metrics were computed for different forecast horizons. The model gris point closest to the buoy location was used to conduct the comparisons.

Models´ intercomparison for the sea surface temperature (using Barcelona II coastal buoy)								
Forecast horizon	**HC01 (-24 h)**		**FC01 (+24 h)**		**FC02 (+48 h)**		**FC03 (+72 h)**	
Metric \ Model	**BCC**	**BCP**	**BCC**	**BCP**	**BCC**	**BCP**	**BCC**	**BCP**
RMSE (°C)	**1.20**	**1.18**	**1.23**	**1.18**	**1.26**	**1.19**	**1.36**	**1.22**
Correlation	**0.97**	**0.98**	**0.97**	**0.98**	**0.97**	**0.98**	**0.96**	**0.98**
Slope	**0.83**	**0.92**	**0.81**	**0.93**	**0.78**	**0.93**	**0.77**	**0.91**

Model Inter-comparison of sea surface height (Barcelona II tide gauge)

In this section, a model intercomparison exercise was performed to evaluate the precision of both coastal circulation models to adequately replicate SSH in situ observations. To this purpose, the model grid point closest to Barcelona II tide gauge was selected to conduct the comparison.

The visual inspection of hourly timeseries revealed that the tide gauge operated adequately, within tolerance ranges, providing quality-controlled data during the 99.7% of the time. Besides, the resemblance between observed and modelled timeseries was relevant during the selected 3-month period, regardless of the forecast horizon used: hindcast (HC01, shown in Figure 12a), +24 h forecast (FC01, Figure 13a), +48 h forecast (FC02, Figure 14a) and +72 h forecast (FC03, Figure 15a). In any case, models were able to qualitatively capture the 38 cm sea level rise (from 0 cm to a peak of 38 cm) that occurred from the 15th to the 20th of October as a result of storm Babet passage (Figure 16a). In the zoomed panel (right side of Figure 12a), it can be seen that BCP outperformed BCC during the peak of the storm. Although the low-pressure core system associated with this storm was cantered over the Bay of Biscay (Figure 16b) and mainly affected the northern Iberian and western French coasts, its remote effect led to a storm surge in the vicinity of Barcelona harbour along with intense south-westerly winds (Figure 16c).

According to the results derived from the best linear fit of scatter plots (shown in Figure 12 b-c, Figure 13 b-c, Figure 14 b-c and Figure 15 b-c), both the slope and the correlation coefficient were always above 0.9. The RMSE values were moderately low, emerging in the range [9.62-10.30] cm.

The skill metrics (gathered in Table 4) revealed that models´ performances were almost identical, with BCP slightly outperforming BCC in terms of lower RMSE, higher correlations coefficients and slope values closer to 1. Again, a gradual (and marginal) loss of precision is observed in both models for longer forecast horizons, but only in terms of slightly higher RMSE values.

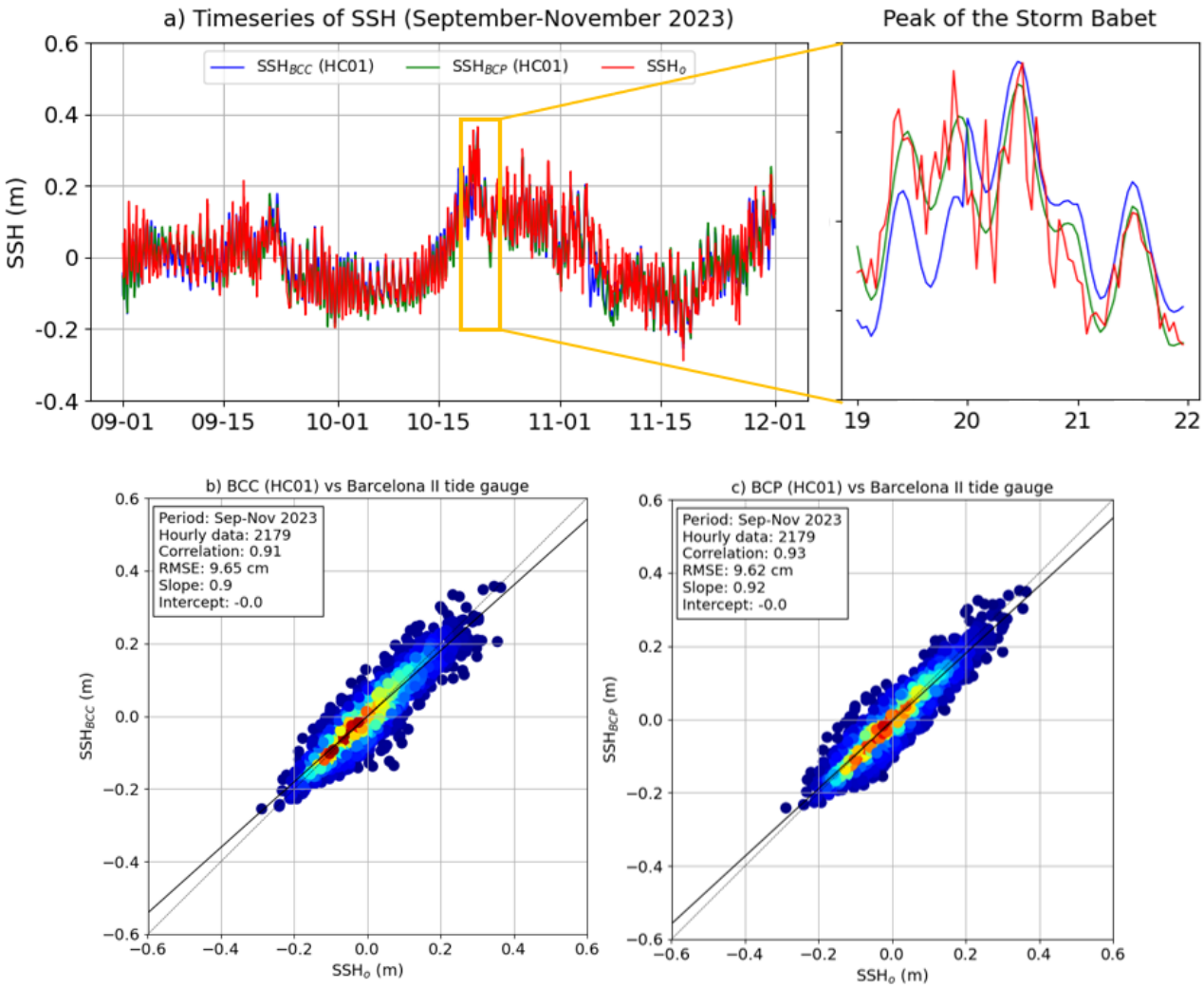

Figure 7. a) Models intercomparison against in situ estimations provided by Barcelona II tide-gauge for a 3-month period (September-November 2023): hourly timeseries of sea surface height from coupled BCC model (SSH_{BCC}, green line), non-coupled BCP model (SSH_{BCP}, blue line) and in situ observations (SSH_o, red line); b) best linear fit (solid black line) of scatter plot between hourly estimations of SSH_{BCC} and SSH_o; c) best linear fit (solid black line) of scatter plot between hourly estimations of SSH_{BCP} and SSH_o. The dotted black line represents the result of perfect agreement with slope 1.0 and intercept 0. Statistical metrics are adhered in white box (upper left corner). In this example, hindcast or best estimates were used (HC01).

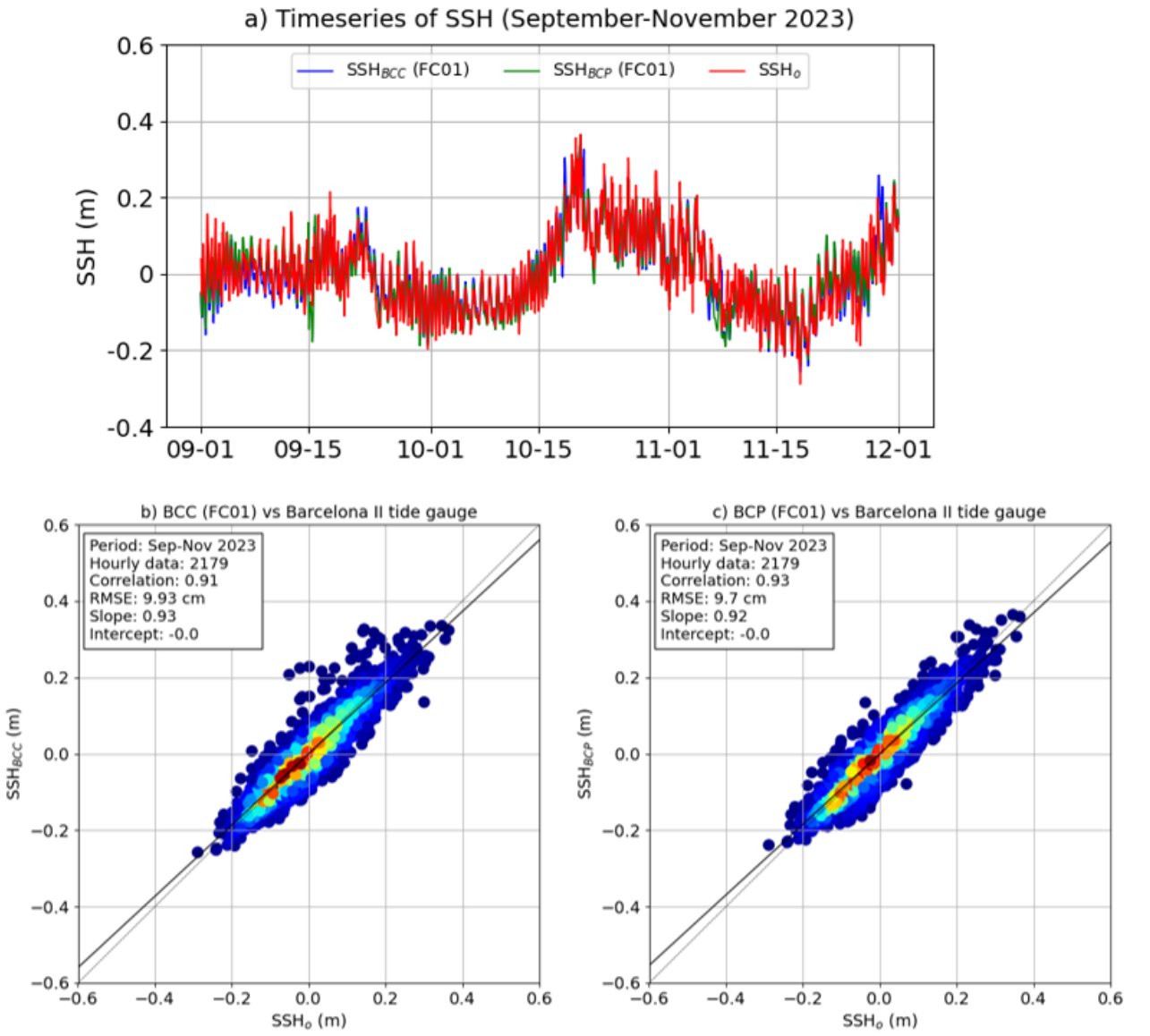

Figure 8. a) Models intercomparison against in situ estimations provided by Barcelona II tide-gauge for a 3-month period (September-November 2023): hourly timeseries of sea surface height from coupled BCC model (SSH$_{BCC}$, green line), non-coupled BCP model (SSH$_{BCP}$, blue line) and in situ observations (SSH$_o$, red line); b) best linear fit (solid black line) of scatter plot between hourly estimations of SSH$_{BCC}$ and SSH$_o$; c) best linear fit (solid black line) of scatter plot between hourly estimations of SSH$_{BCP}$ and SSH$_o$. The dotted black line represents the result of perfect agreement with slope 1.0 and intercept 0. Statistical metrics are adhered in white box (upper left corner). In this example, the +24 h forecast horizon was used (FC01).

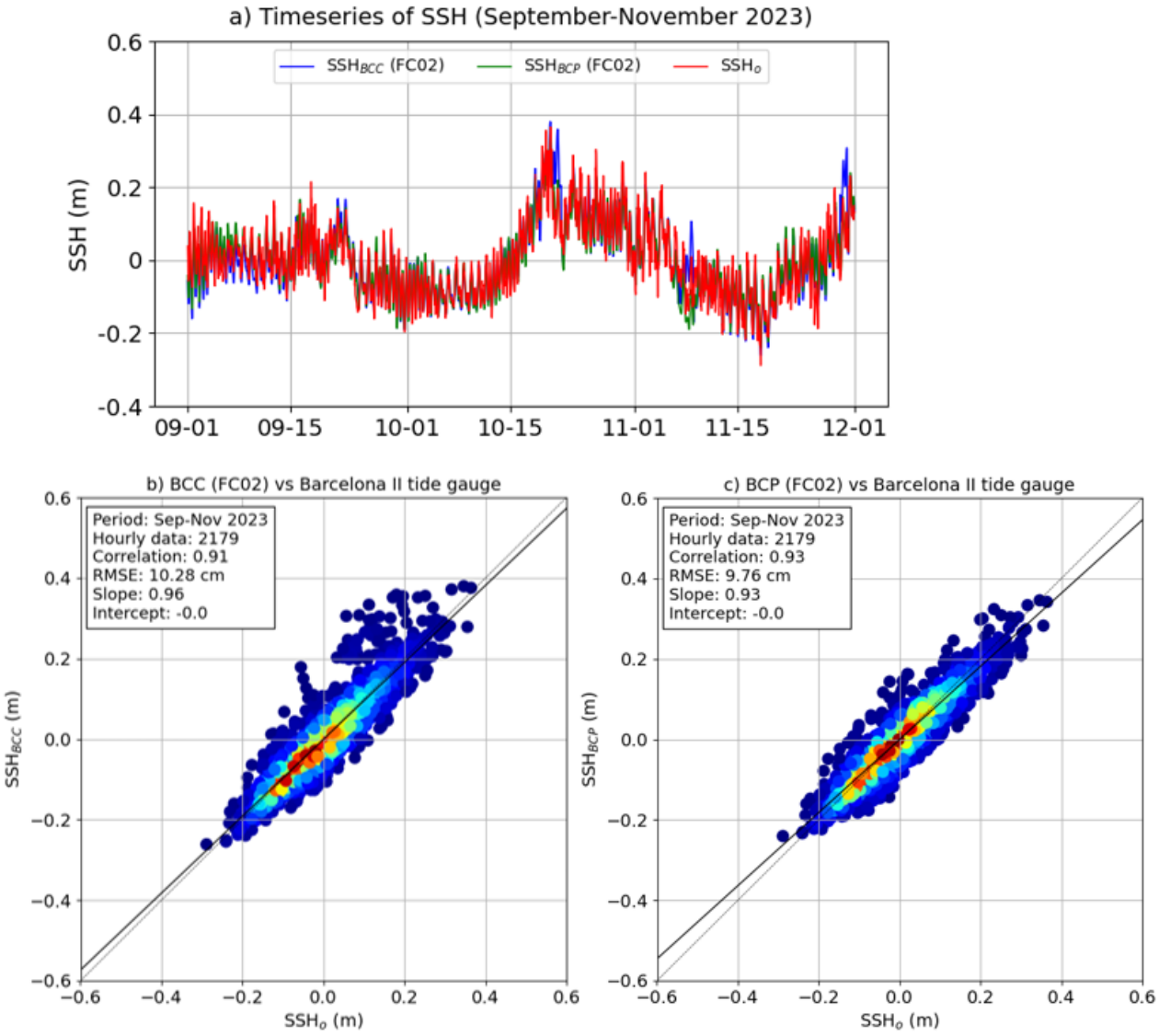

Figure 9. Models intercomparison against in situ estimations provided by Barcelona II tide-gauge for a 3-month period (September-November 2023): hourly timeseries of sea surface height from coupled BCC model (SSH$_{BCC}$, green line), non-coupled BCP model (SSH$_{BCP}$, blue line) and in situ observations (SSH$_o$, red line); b) best linear fit (solid black line) of scatter plot between hourly estimations of SSH$_{BCC}$ and SSH$_o$; c) best linear fit (solid black line) of scatter plot between hourly estimations of SSH$_{BCP}$ and SSH$_o$. The dotted black line represents the result of perfect agreement with slope 1.0 and intercept 0. Statistical metrics are adhered in white box (upper left corner). In this example, the +48 h forecast horizon was used (FC02).

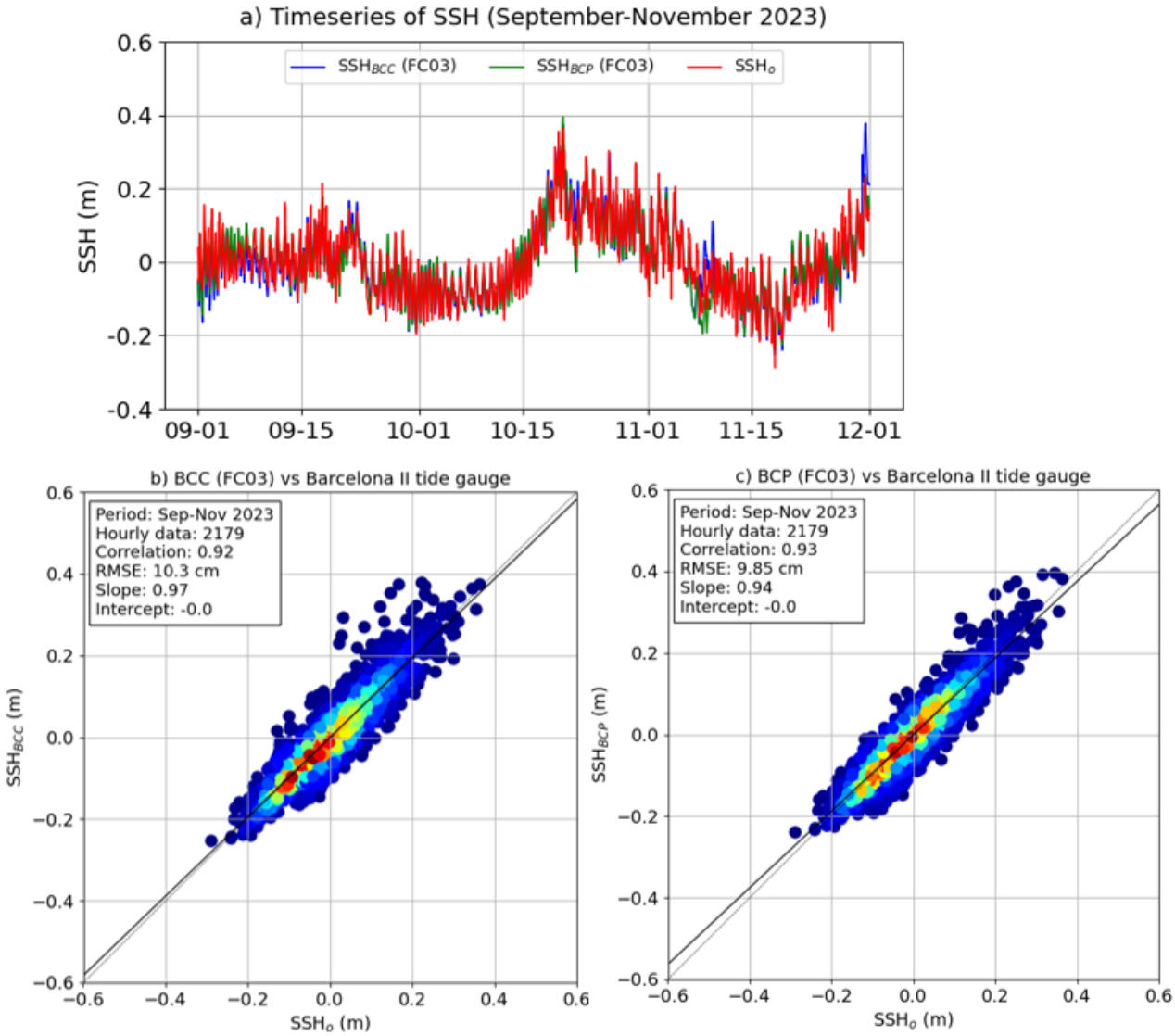

Figure 10. a) Models intercomparison against in situ estimations provided by Barcelona II tide-gauge for a 3-month period (September-November 2023): hourly timeseries of sea surface height from coupled BCC model (SSH$_{BCC}$, green line), non-coupled BCP model (SSH$_{BCP}$, blue line) and in situ observations (SSH$_o$, red line); b) best linear fit (solid black line) of scatter plot between hourly estimations of SSH$_{BCC}$ and SSH$_o$; c) best linear fit (solid black line) of scatter plot between hourly estimations of SSH$_{BCP}$ and SSH$_o$. The dotted black line represents the result of perfect agreement with slope 1.0 and intercept 0. Statistical metrics are adhered in white box (upper left corner). In this example, the +72 h forecast horizon was used (FC03).

Table 4. Summary of metrics derived from the models intercomparison of sea surface height (SSH) against in situ estimations provided by Barcelona II tide gauge for the 3-month period September-November 2023. The metrics were computed for different forecast horizons. The model gris point closest to the tide-gauge location was used to conduct the comparisons.

Models´ intercomparison for the sea surface height (using Barcelona II tide gauge)								
Forecast horizon	**HC01 (-24 h)**		**FC01 (+24 h)**		**FC02 (+48 h)**		**FC03 (+72 h)**	
Metric \ Model	**BCC**	**BCP**	**BCC**	**BCP**	**BCC**	**BCP**	**BCC**	**BCP**
RMSE (cm)	**9.65**	**9.62**	**9.93**	**9.70**	**10.28**	**9.76**	**10.30**	**9.85**
Correlation	**0.91**	**0.93**	**0.91**	**0.93**	**0.91**	**0.93**	**0.92**	**0.93**
Slope	**0.90**	**0.92**	**0.93**	**0.92**	**0.96**	**0.93**	**0.97**	**0.94**

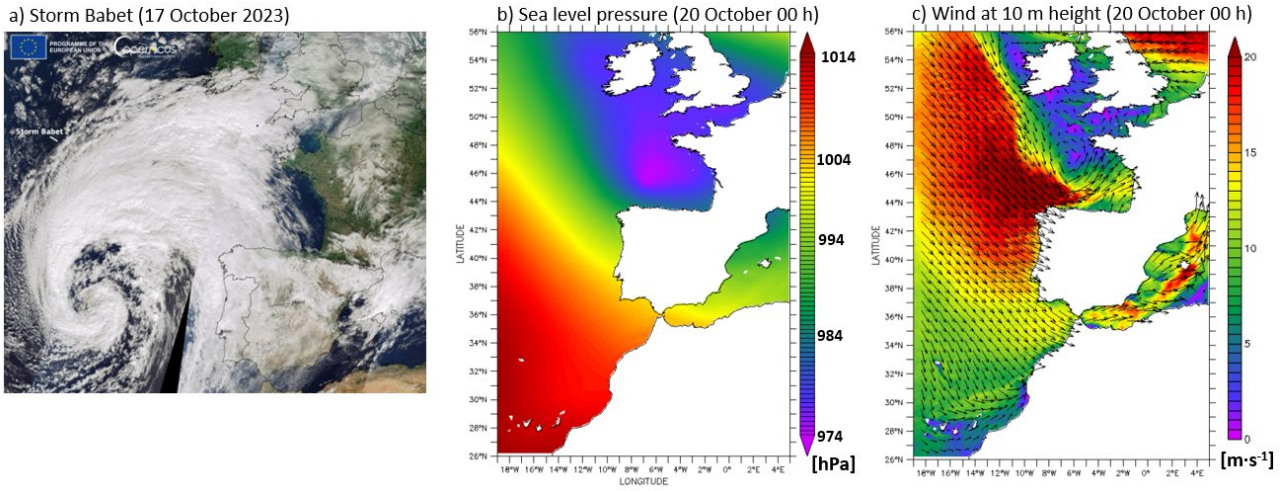

Figure 11. Storm Babet (16-21 October 2023). a) Snapshot of satellite image map showing the cloud clover, as provided by the Copernicus Service; b-c) hourly maps of sea level pressure and the associated wind at 10 m height, as provided by the ECMWF.

Model Inter-comparison of sea surface height (RAD1 and RAD2 tide gauges)

In this section, a model intercomparison exercise similar to that conducted in the previous section was performed. In this case, we used SSH dataset provided by two new radar sensors installed within the frame of EuroSea project. Therefore, the main goal is to showcase the monitoring capability of the new instrumentation. Again, the model grid point closest to RAD1 and RAD2 sensors was selected to conduct the comparison.

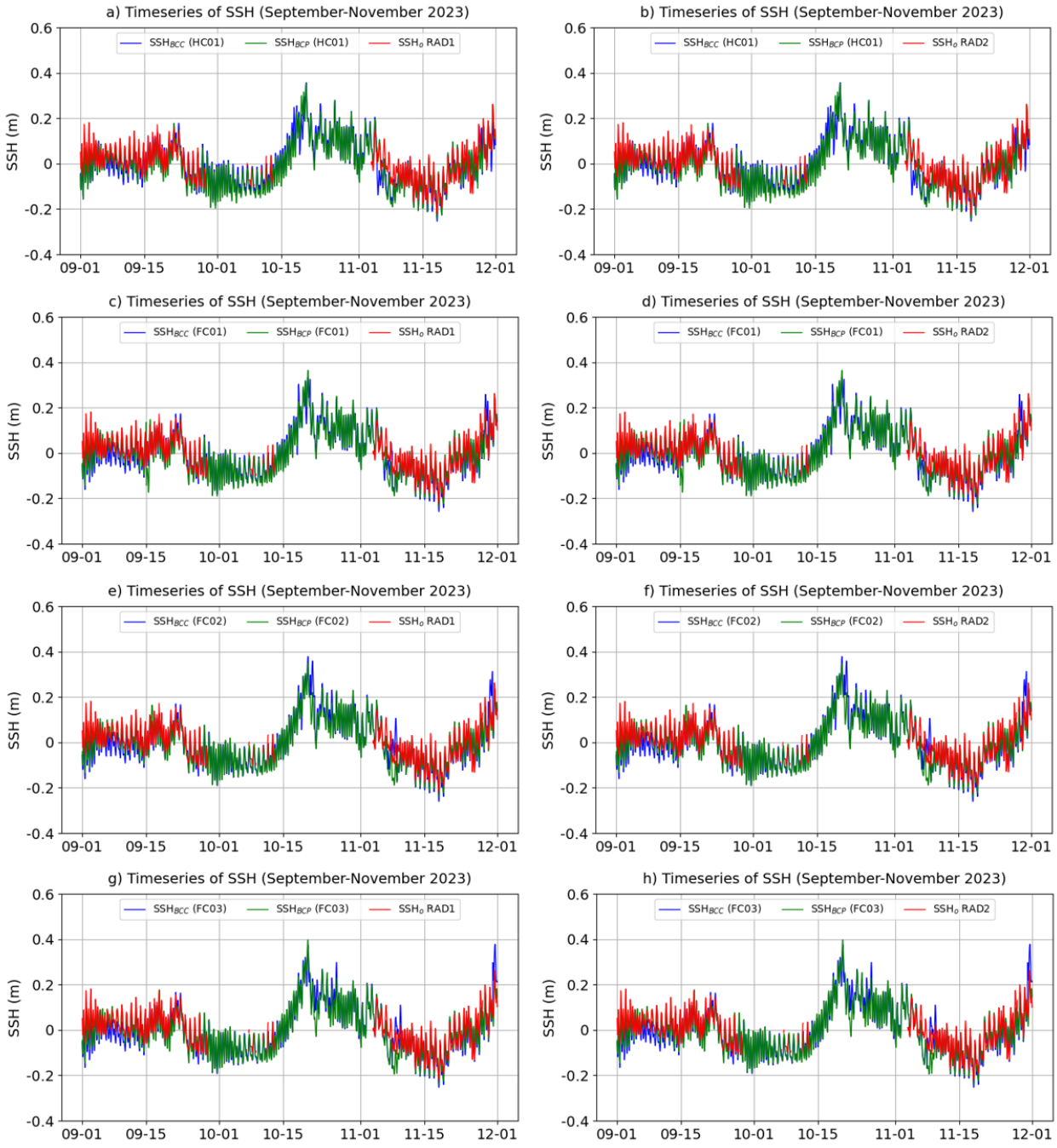

Figure 12. Models intercomparison against in situ estimations provided by RAD1 (left) and RAD2 (right) tide-gauges for a 3-month period (September-November 2023): hourly timeseries of sea surface height from coupled BCC model (SSH_{BCC}, green line), non-coupled BCP model (SSH_{BCP}, blue line) and in situ observations ($SSH_{o,}$, red line) for different forecast horizons: HC01 (a-b), FC01 (c-d), FC02 (e-f) and FC03 (g-h).

The exploration of hourly timeseries revealed that both sensors suffered from a temporal outage that comprised the entire month of October, so data provision was around the 65% for the 3-month period selected. Notwithstanding, the visual resemblance between observed and modelled timeseries was relevant, independently of the forecast horizon analysed: hindcast (HC01, shown in Figure 17 a-b), +24 h forecast (FC01, Figure 17 c-d), +48 h forecast (FC02, Figure 17 e-f) and +72 h forecast (FC03, Figure 17 g-h).

The skill metrics for RAD1 sensor (Table 5) and RAD2 sensor (Table 6) were exactly the same. Once again, results revealed that models´ performances were rather similar, with BCP slightly outperforming BCC in terms of lower RMSE. Correlations coefficients and slope values were of the same order. Again, a gradual (and marginal) loss of precision is observed in both models for longer forecast horizons, but only in terms of slightly higher RMSE values.

Table 5. Summary of metrics derived from the models intercomparison of sea surface height (SSH) against in situ estimations provided by RAD1 tide gauge for the 3-month period September-November 2023. The metrics were computed for different forecast horizons. The model grid point closest to the tide-gauge location was used to conduct the comparisons.

Models´ intercomparison for the sea surface height (using RAD1 tide gauge)								
Forecast horizon	**HC01 (-24 h)**		**FC01 (+24 h)**		**FC02 (+48 h)**		**FC03 (+72 h)**	
Metric \ Model	**BCC**	**BCP**	**BCC**	**BCP**	**BCC**	**BCP**	**BCC**	**BCP**
RMSE (cm)	**8.29**	**8.27**	**8.65**	**8.31**	**8.69**	**8.34**	**8.78**	**8.38**
Correlation	**0.88**	**0.90**	**0.88**	**0.90**	**0.88**	**0.90**	**0.88**	**0.90**
Slope	**0.91**	**0.94**	**0.96**	**0.95**	**0.95**	**0.95**	**0.96**	**0.96**

Table 6. Summary of metrics derived from the models intercomparison of sea surface height (SSH) against in situ estimations provided by RAD2 tide gauge for the 3-month period September-November 2023. The metrics were computed for different forecast horizons. The model grid point closest to the tide-gauge location was used to conduct the comparisons.

Models´ intercomparison for the sea surface height (using RAD2 tide gauge)								
Forecast horizon	**HC01 (-24 h)**		**FC01 (+24 h)**		**FC02 (+48 h)**		**FC03 (+72 h)**	
Metric \ Model	**BCC**	**BCP**	**BCC**	**BCP**	**BCC**	**BCP**	**BCC**	**BCP**
RMSE (cm)	**8.29**	**8.27**	**8.65**	**8.31**	**8.69**	**8.34**	**8.78**	**8.38**
Correlation	**0.88**	**0.90**	**0.88**	**0.90**	**0.88**	**0.90**	**0.88**	**0.90**
Slope	**0.91**	**0.94**	**0.96**	**0.95**	**0.95**	**0.95**	**0.96**	**0.96**

Qualitative model inter-comparison during a coastal upwelling event

Coastal upwelling, which is a process that modulate the connectivity between offshore waters and coastal ecosystems, has been extensively studied along the Iberian Peninsula coastline (Lorente et al., 2020). It occurs when alongshore winds and the Coriolis effect (due to Earth's rotation) combine to drive a near-surface layer of water offshore, a process referred to as Ekman transport (Ekman, 1905). Such cross-shelf transport is compensated for by the vertical uplift of cold and enriched waters that fertilize the uppermost layer and foster high marine productivity.

As previously shown in section 4.1, there was a significant drop of SST during late October- early November 2023 that was properly captured by the two coastal models analysed in the present document. The aim of

this subsection is to gain further insight into the modelled surface current that drove this coastal phenomenon of paramount importance. Since there were no instrumental platforms (current meters or Acoustic Doppler Current Profilers) available in the study area to be used as ground truth, we employed two independent Copernicus satellite missions to assess the consistency of the modelled surface circulation and infer if these model outcomes are in line with well-known aspects of the coastal upwelling process.

The daily satellite-derived maps of SST and CHL (Figure 18) exhibited the effects of intense south-westerly winds (Figure 16c) over the surface layer in the NW Mediterranean Sea. A steady cooling (below 17°C) along the entire Levantine coastline is evidenced (Figure 18 a-d), with surrounding warmer waters reaching up to 20-22°C. Concomitant peaks of CHL (above 0.8 mg·m^{-3}) were detected close to the eastern Iberian shoreline, thus suggesting accrued injection of subsurface nutrients (Figure 18, e-h) in the same areas where the sharp cooling was taken place, as usually observed during typical upwelling conditions.

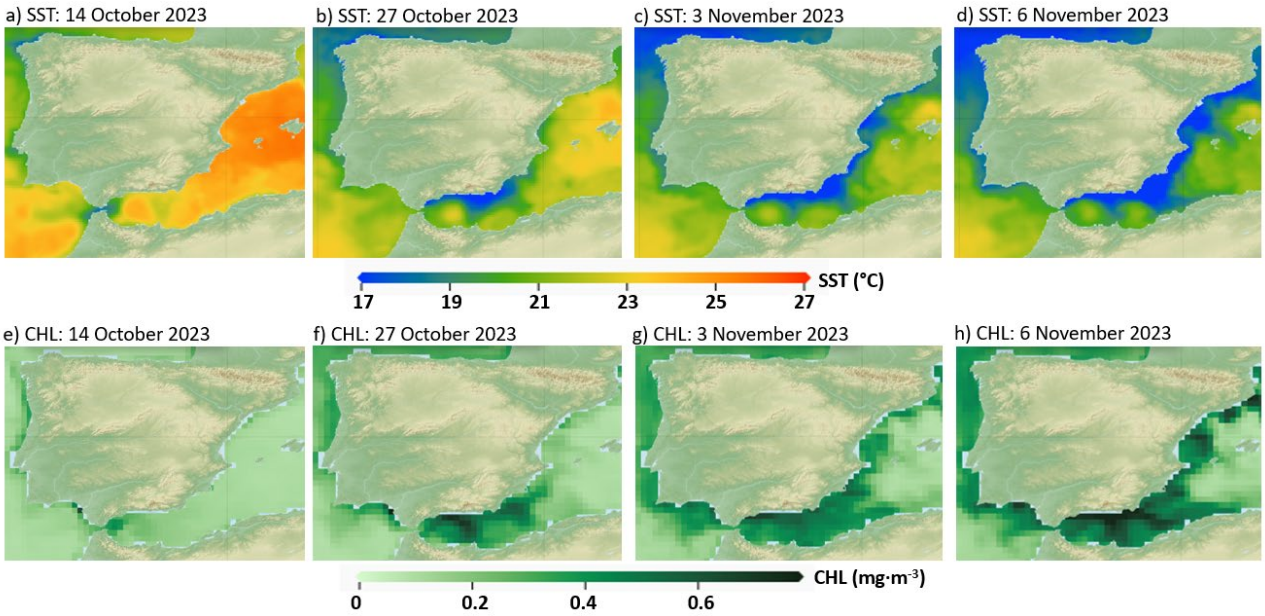

Figure 13. a-d) Daily satellite-derived maps of sea surface temperature (SST) and e-h) chlorophyll concentration (CHL), as provided by the Copernicus Service.

The prognostic capabilities of both BCP and BCC coastal circulation models to reproduce this intense and long-lasting upwelling event in the vicinity of Barcelona harbour were assessed. From a qualitative perspective, the daily maps of surface circulation presented similar patterns (Figure 19), namely: the rather uniform offshore deflection of the main surface flow during upwelling favourable conditions due to predominant SW winds (27th of October, shown in Figure 19 a-b) and westerly winds (3rd of November, Figure 19 c-d).

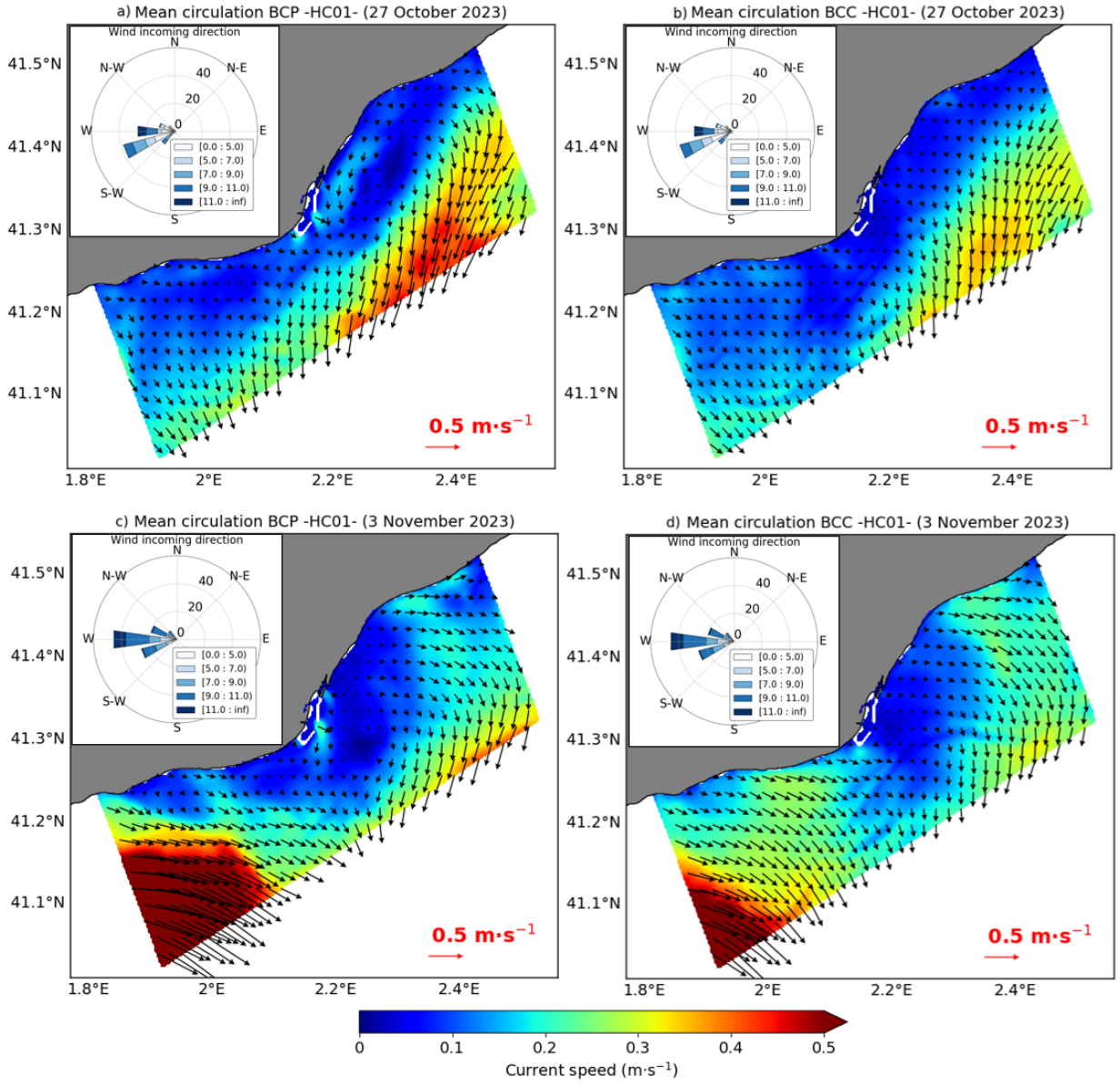

Figure 14. (a-b) Daily maps of surface circulation in the vicinity of Barcelona harbour during predominant south-westerly winds (recorded by a meteorological station installed within the harbour), as modelled by non-couple BCP model (a) and wave-current coupled BCC model (b); (c-d) Idem, under predominant intense westerlies.

This modelled surface circulation patterns are in close agreement with previously reported aspects of coastal upwelling. Both models were also capable of reproducing the wind-driven south-westward flow that is usually observed under the action of NE winds (Figure 20) commonly known as the North Current. This quasi-permanent SW flow is only altered by clockwise inertial oscillations (with maximum occurrence during the warm stratified season) and some short periods of current reversals (line the one here studied), related to mesoscale events like frontal instabilities, meanders, eddies and filaments (Grifoll et al., 2015).

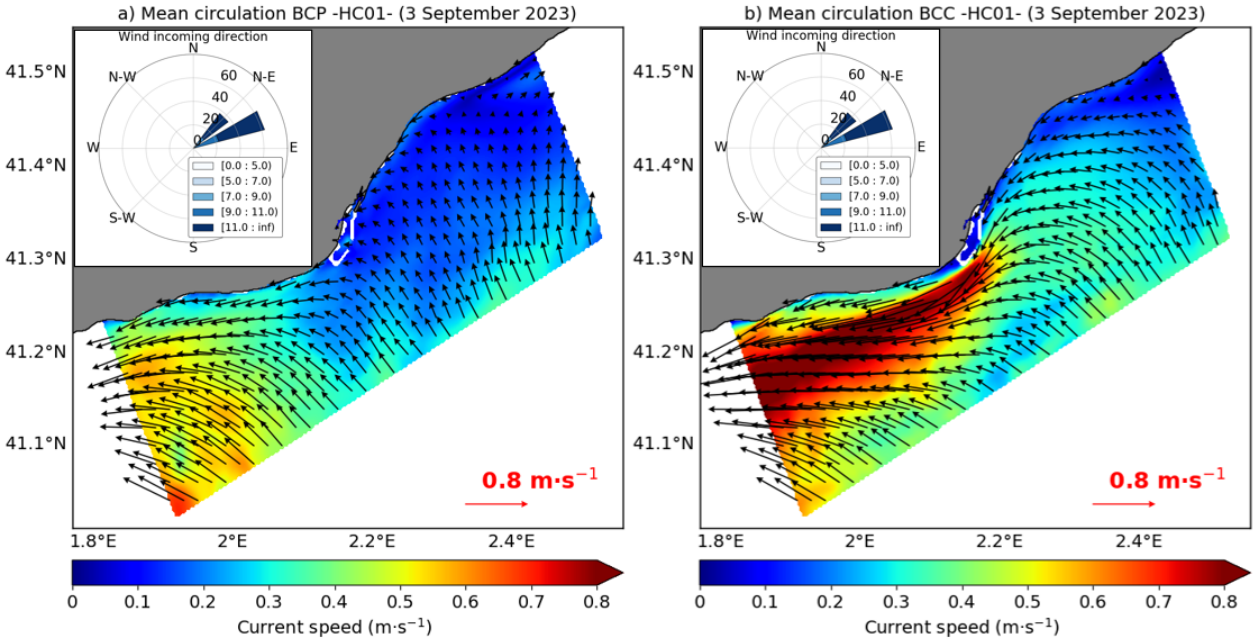

Figure 15. Daily maps of surface circulation in the vicinity of Barcelona harbour during predominant north-easterly winds (recorded by a meteorological station installed within the harbour), as modelled by non-couple BCP model (a) and wave-current coupled BCC model (b).

5.2. Taranto pilot site

The model data are based on operational forecasting. The evaluation of the model's performance involves assessing its skill by comparing the first day of forecast with newly observed data, as outlined in section 2.2.

In consideration of data availability, this report presents the time series of sea level (Figure 21) and significant wave height (Figure 22), along with the corresponding BIAS and RMSE values against the observations.

For sea level, an RMSE of 3.2 cm is highlighted over the entire time series; this result is comparable to the findings presented in the hindcast simulation described in D5.3.

Regarding the significant wave height (SWH), the model results are compared with two different sensors (MIROS and GNSS-IR as described in section 2.2.). The model demonstrates satisfactory agreement, showing an RMSE of 5.2cm and 7.8cm over the entire time series for the two datasets. Notably, the model overestimates the first peak on October 22, 2023, by about 18% (0.78 cm vs. 0.64 cm for MIROS), while exhibiting good agreement during the subsequent period especially for MIROS.

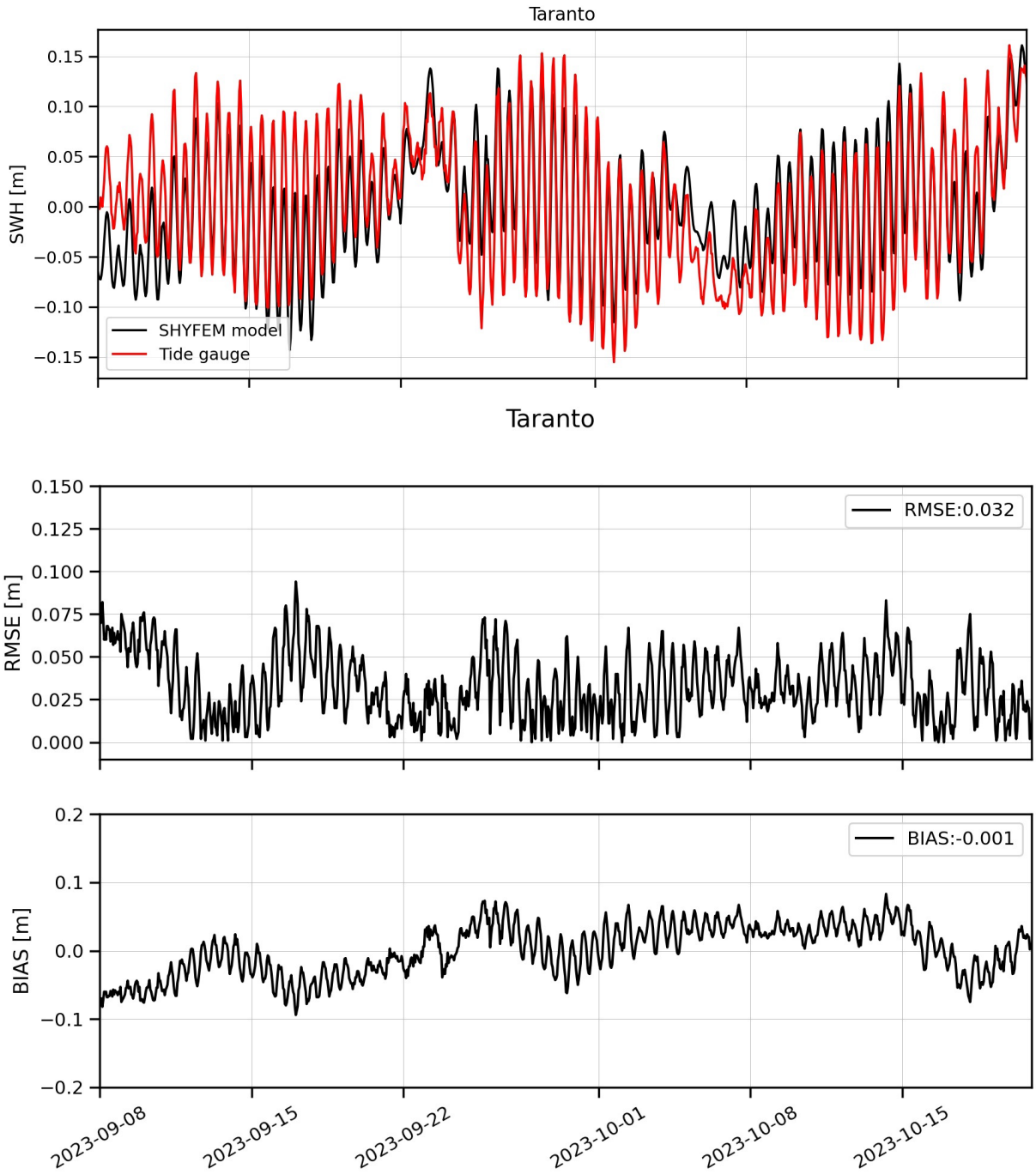

Figure 21: Model timeseries of sea level for the 1st day of forecast compared with the observation (upper panel). RMSE and BIAS are reported in central and lower panels.

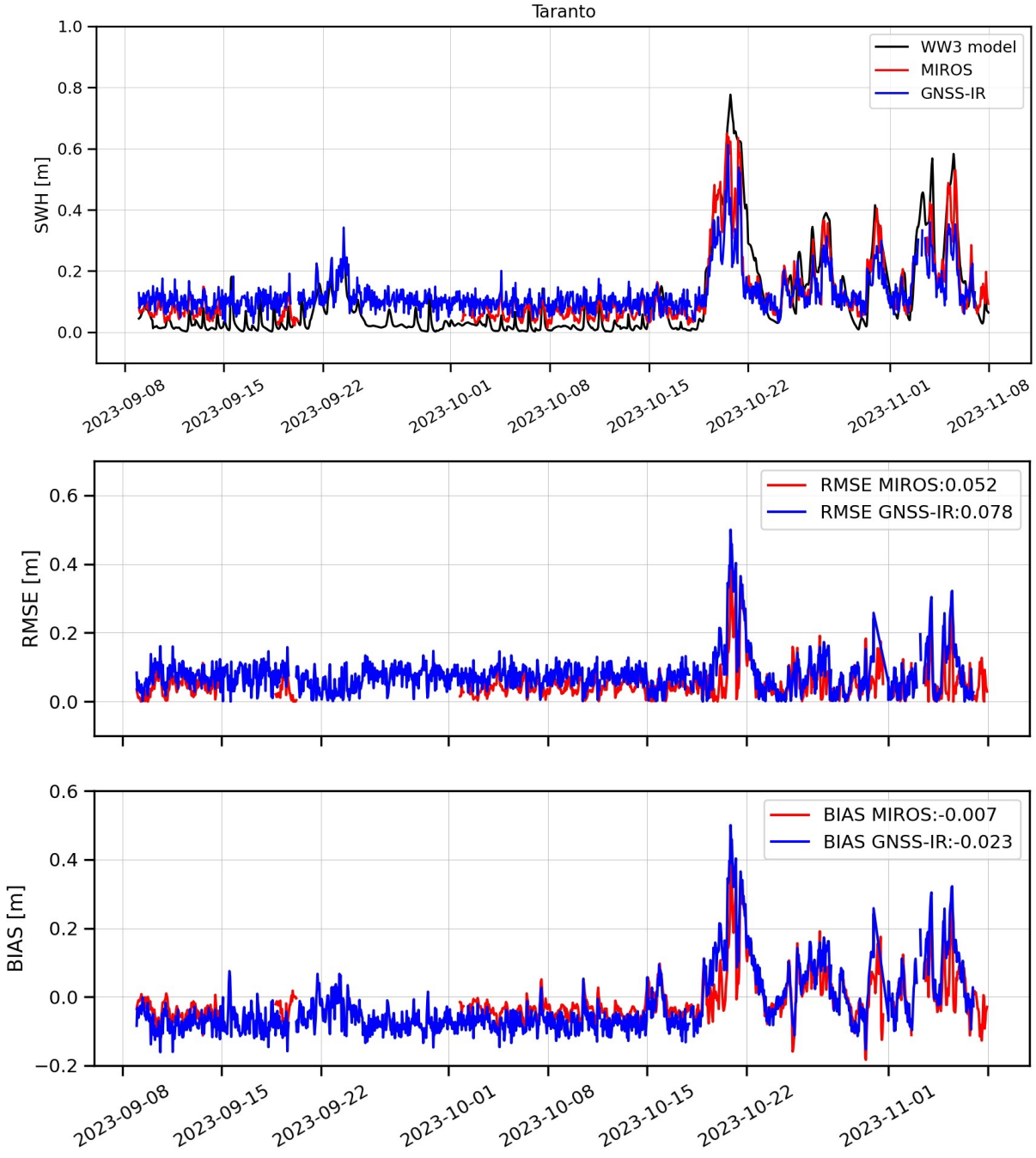

Figure 22: Model timeseries of significant wave height for the 1st day of forecast compared with the observation (upper panel). RMSE and BIAS are reported in central and lower panels.

Conclusions

The skills assessment of the high-resolution coastal models developed in the frame of the OSPAC demonstrator for Barcelona and Taranto pilot sites has confirmed their good performance during the demonstration phase (August-December 2023), when compared with observational data from the new sensors deployed, or from other permanent stations (in the case of Barcelona). This result is in general agreement with the offline validation exercises presented for other data periods in D5.3 and D5.4. In both cases, the exercise also confirmed the potential of the new GNSS-IR technique to provide valuable significant wave height values at the coast, both by the use of a low cost GNSS sensor installed in Barcelona, or the higher-precision and more precise GNSS station, also used for sea level measurements and vertical land motion, of the EuroSea tide gauge in the case of Taranto.

A more comprehensive study was conducted in this report for the Barcelona pilot site, where the availability of two operational coastal models, with and without waves-currents coupling, and more in situ observations, has allowed a first insight on the benefits of the new coupled approach.

A 6-month (June-November 2023) characterization of the wave regime affecting Barcelona harbour (NW Mediterranean Sea) was conducted. To this aim, quality-controlled wave estimations and high-resolution model predictions were used in concert on an hourly basis. The results revealed that the prevailing incoming wave direction was in the SW-S sector. Equally, skill metrics indicated that model performance was consistent (correlation coefficients above 0.85) with a variety of sea states despite overestimating the most relevant wave height events. An additional factor that might contribute to the discrepancies observed in SWH in this region consists of the hydrodynamic modulations of waves by periodic underlying currents so further investigation on waves–current interaction should be undertaken in the future. Finally, the low-cost GNSS sensor was proved to be a sound and cheap remote sensing tool to retrieve wave information in port-approach areas, although significant gaps in the data provision were evidenced during the experiment, due to power failure issues that are now being solved by NOC and the port. Overall, these results demonstrate that a synergistic observational and modelling approach can provide a comprehensive characterization of wave conditions in coastal areas and show benefit from the complementary nature of both systems.

A 3-month (September-November 2023) multi-parameter intercomparison was conducted for two coastal ocean models running operationally around Barcelona harbour (NW Mediterranean Sea). To this aim, quality-controlled estimations of sea surface temperature and sea water level, along with high-resolution model predictions, were used in concert on an hourly basis. In addition, ancillary datasets were used to qualitatively evaluate the consistency of both models' outcomes. The results revealed that the two coastal ocean forecast system worked robustly, within tolerance ranges, for the selected study period, being able to adequately capture specific events like the sea level rise associated with the passage of Storm Babet or the water cooling related to a prolonged upwelling episode occurred under intense SW winds. However, there are some aspects that deserve a detailed explanation such as the fact that the coupled BCC model was not able to outperform the non-coupled BCP model. As coupled models have been reported to capture important physics of the wave-current interaction under very different scales and environmental conditions, we consider that the 3-month period selected was clearly insufficient. Therefore, a complementary model intercomparison exercise covering an entire annual cycle should be conducted in the short-term future to gain further insight. An additional factor that could partially explain these results is the absence of any relevant wave storm directly affecting in the western Mediterranean. Wintertime extreme events, commonly

observed in the Gulf of Lion and adjacent areas of the NW Mediterranean, could aid to better analyse the behaviour of the coupled model under a broad range of metocean conditions.

References

Bellafiore, D., Umgiesser, G.: Hydrodynamic coastal processes in the north Adriatic investigated with a 3D finite element model, Ocean Dynam., 60, 255–273, 2010.

Booij, N., Ris, R.C., Holthuijsen, L.H.: A third-generation wave model for coastal regions. Part I: Model description and validation. Journal of Geophysical Research 104 (C4), 7649–7666., 1999.

Copernicus Marine In situ Team: Copernicus in Situ TAC, Real Time Quality Control for WAVES. Toulouse, France: Copernicus in situ TAC, 1–19. doi:10.13155/46607, 2017.

Dobricic, S., and N. Pinardi: An oceanographic three-dimensional variational data assimilation scheme. Ocean Modell., 22, 89–105, 2008.

Ekman, W.: On the influence of the Earth's rotation on ocean currents, Ark. Mat. Astr. Fys., 2, 1–52, 1905.

Emery, W.J. and Thompson, R.E. Data Analysis Methods in Physical Oceanography, Elsevier Science, ISBN 9780080477008, 654 pages, Amsterdam, 2001.

Ferrarin, C., Roland, A., Bajo, M., Umgiesser, G., Cucco, A., Davolio, S., Buzzi, A., Malguzzi, P., Drofa, O.: Tide-surge-wave modelling and forecasting in the Mediterranean Sea with focus on the Italian coast, Ocean Model., 61, 38–48, 2013.

Grifoll, M., Aretxabaleta, A. L., and Espino, M.: Shelf response to intense offshore wind. J. Geophys. Res. Oceans 120, 6564–6580. doi: 10.1002/ 2015jc010850, 2015.

Haidvogel, D. B. , Arango, H.G., Budgell, W. P., Cornuelle, B. D., Curchitser, E., Di Lorenzo, E., Fennel, K., Geyer, W. R., Hermann, A. J., Lanerolle, L., Levin, J., McWilliams, J. C., Miller, A. J., Moore, A. M., Powell, T. M., Shchepetkin, A. F., Sherwood, C. R., Signell, R. P., Warner, J. C., Wilkin, J.: Ocean forecasting in terrain-following coordinates: Formulation and skill assessment of the Regional Ocean Modeling System, Journal of Computational Physics. 227, 3595-3624, 2008.

Jacob, R., Larson, J. and Ong, E.: M×N communication and parallel interpolation in community climate system model version 3 using the model coupling toolkit, The International Journal of High Performance Computing Applications, 19(pp), 277–292, 2005.

Komen, G. J., S. Hasselmann and K. Hasselmann: On the existence of a fully developed wind-sea spectrum. J. Phys. Oceanogr., 14, 1,271–1,285, 1984.

Korres, G., Ravdas, M., Zacharioudaki, A., Denaxa, D., & Sotiropoulou, M.: Mediterranean Sea Waves Analysis and Forecast (CMEMS MED-Waves, MedWAM3 system) (Version 1) set. Copernicus Monitoring Environment Marine Service (CMEMS), 2021 https://doi.org/10.25423/CMCC/MEDSEA_ANALYSISFORECAST_WAV_006_017_MEDWAM3.

Lorente, P., Piedracoba, S., Montero, P., Sotillo, M.G., Ruiz, M.I. and Álvarez-Fanjul, E.: Comparative analysis of summer upwelling and downwelling events in NW Spain: a model-observations approach, Remote Sens., 12, 2762, https://doi.org/10.3390/rs12172762, 2020.

Madec, G.: NEMO ocean engine, Note du Pole de modelisation, Institut Pierre-Simon Laplace (IPSL), France, 27, 1288–1619, 2008.

Micaletto, G., Barletta, I., Mocavero, S., Federico, I., Epicoco, I., Verri, G., Coppini, G., Schiano, P., Aloisio, G., and Pinardi, N.: Parallel implementation of the SHYFEM (System of HydrodYnamic Finite Element Modules) model, Geosci. Model Dev., 15, 6025–6046, https://doi.org/10.5194/gmd-15-6025-2022, 2022.

Pérez Gómez, B., Vela, J., and Alvarez Fanjul, E.: A new concept of multi- purpose sea level station: example of implementation in the REDMAR network. In: Proceedings of the Fifth International Conference on EuroGOOS, May 2008: Coastal to global operational oceanography: achievements and challenges, Exeter, 2008.

Pérez Gómez, B., A. Payo, D. López, P.L. Woodworth and E. Alvarez Fanjul: Overlapping sea level time series measured using different technologies: an example from the REDMAR Spanish network. Nat. Hazards Earth Syst. Sci., 14, 589-610, 2014.

Pugh, D.T.: Tides, Surges and Mean Sea level. Chichester: John Wiley and Sons, 472 pp, 1987.

Sánchez-Arcilla, A., González-Marco, D., and Bolaños, R.: A review of wave climate and prediction along the Spanish Mediterranean coast. Nat. Hazards Earth Syst. Sci. 8, 1217–1228. doi: 10.5194/nhess-8-1217-2008, 2008.

Shchepetkin, A. F., McWilliams, J.C.: The Regional Oceanic Modeling System: A split-explicit, free-surface, topography-following coordinate oceanic model. Ocean Modeling 9, 347–404 doi:10.1016/j.ocemod.2004.08.002, 2005.

Shchepetkin, A. F., McWilliams, J. C.: Correction and commentary for “Ocean forecasting in terrain-following coordinates: Formulation and skill assessment of the regional ocean modeling system” by Haidvogel et al., J. Comp. Phys. 227, pp. 3595–3624.”. Journal of Computational Physics. 228, 8985-9000. 2009.

Umgiesser, G., Canu, D. M., Cucco, A., Solidoro, C.: A finite element model for the Venice lagoon: Development, set up, calibration and validation, J. Marine Syst., 51, 123–145, 2004.

Umgiesser, G., Ferrarin, C., Cucco, A., De Pascalis, F., Bellafiore, D., Ghezzo, M., Bajo, M.: Comparative hydrodynamics of 10 Mediterranean lagoons by means of numerical modeling, J. Geophys. Res.-Oceans, 119, 2212–2226, 2014.

Warner, J.C., Armstrong, B., He, R., and Zambon, J.: Development of a Coupled Ocean-Atmosphere Wave-Sediment Transport (COAWST) Modeling System. Ocean Modelling, 35, 230-244, 2010.